Synthesis of diamonds by use of microwave plasma chemical-vapor deposition: Morphology and growth of diamond films

Koji Kobashi, Kozo Nishimura, Yoshio Kawate, and Takefumi Horiuchi
Electronics Technology Center, Kobe Steel, Ltd., 1-5-5 Takatsukadai, Nishi-ku, Kobe 673-02, Japan
(Received 15 January 1988)

An investigation is made of the surface morphology and growth of polycrystalline diamond films deposited on Si substrates using the microwave plasma chemical-vapor-deposition (CVD) method. For the source gas, CH_4 and H_2 gases mixed in different concentrations are used. Scanning electron microscope pictures of the diamond films synthesized for 7 h show that the film surface consists of triangular (111) diamond faces for CH_4 concentrations $c < 0.4$ vol %, whereas square (100) faces are predominant above $c \simeq 0.4$ vol %. For $c > 1.2$ vol %, the number density of (100) faces decreases with c and finally at $c \simeq 1.6$ vol % the film surface becomes entirely structureless, consisting of microcrystallites only. For characterization of the films, x-ray and electron diffraction are measured along with Raman and infrared spectra. In the study of the evolution of surface morphology during film growth, it is found that diamond particles grown on the substrate initially increase their size almost uniformly until the substrate is entirely covered. Then a secondary growth takes place, followed by surface-restructuring processes such as "fusion" and "absorption" among secondary crystallites. As a result, well-defined diamond faces are formed progressively on the film surface. Higher-order growths followed by the restructuring processes occur periodically as the CVD synthesis proceeds.

I. INTRODUCTION

During the past few years, significant progress has been made on experimental techniques for synthesizing diamonds by the decomposition of hydrocarbon gases. Particularly notable is the finding by Setaka and colleagues[1] that, using three different chemical-vapor-deposition (CVD) methods, diamonds can be grown from a methane-hydrogen mixed gas on various substrates such as Si, and of course on bulk diamonds, at a rate of about 0.2–0.5 μm/h. X-ray and electron diffraction, Raman scattering, and other analyses indicate that the properties of the CVD diamonds are very similar to those of impurity-free, type-IIa bulk diamond. In this respect, the CVD diamonds are clearly distinct from the amorphous hydrogenated carbon (a-C:H) which is often called i-C or diamondlike carbon (DLC). This finding instigated extensive research on the CVD syntheses of diamonds in Japan, and more recently also in the United States, aimed at the applications of the CVD diamonds to abrasive coatings, heat sinks, and high-performance electronic devices. In the following, the history and current status of the synthesis of diamonds using CVD techniques will be briefly reviewed for readers not familiar with this research field, as no such work is available so far.

Attempts for man-made diamonds have been made since the 19th century, and a new era was opened up in 1954 by Bundy and co-workers,[2] who established the high-pressure–high-temperature (HP-HT) technology for diamond synthesis. After three decades of extensive studies, the following methods have been established: (1) direct conversion from graphite to diamond using shock waves, (2) direct conversion under HP-HT conditions, (3) HP-HT conversion using metal solvents, and finally (4) deposition of diamonds on substrates from hydrocarbon gases. A characteristic of the gas-phase synthesis (4) is that the thermodynamic conditions in the synthesis are favorable for graphite, and diamond is only metastable. Therefore, co-deposition of graphite has to be suppressed by atomic hydrogen excessively present in the reaction chamber, as will be described later. This is in strong contrast to the shock-wave and HP-HT methods in which diamond is thermodynamically more stable than graphite in the conversion processes.

It is well known that diamond has a number of excellent properties:[3,4] most important, it is the hardest material known. The elastic constant is large (107.6×10^{11} dyn/cm^2), but the specific density is small (3.31 g/cm^3). Also the thermal expansion coefficient is small (4.50×10^{-6} K^{-1} at 750 °C). Optically, it is transparent from the infrared to the visible region, and the refractive index is as large as 2.417. The thermal conductivity of type-IIa diamond (20 W/cm K) is the highest of all materials at room temperature, about 5 times larger than the value for Cu. Electrically, it is a good insulator and the band gap associated with the indirect transition between the covalent and conduction bands is as large as 5.47 eV. The dielectric constant is small ($n = 5.58$). Diamond is chemically inert and resistant to high temperatures, particularly in an oxygenless environment. It is also resistant to x radiation, γ radiation, ultraviolet light, and nuclear particles.

Diamonds synthesized by CVD have all these properties,[5] and moreover, either p- or n-type diamond films can be formed on substrates simply by mixing impurity gases such as diborane (B_2H_6) or phosphine (PH_3), respective-

ly, in the reactant gas.[6] It is thus expected that diamond films have a vast area of applications, particularly in the field of electronics, and this is why the gas-phase synthesis has attracted so much attention recently. Perhaps our final goal is to synthesize single-crystalline diamond films with controlled dopings for microelectronic devices. Such a field may be called diamond electronics.

The first successful diamond synthesis from the gas phase was reported by Eversole in 1958.[7] In this method, a carbon-containing gas was passed over seed crystals (diamond powder) at a temperature of around 1000 °C and a pressure of a few Torr. New diamond was formed on the seeds until it was hampered by the accumulation of black carbon (graphite and *a*-C), which was then removed by heating the diamond-deposited seed crystals in hydrogen gas at about 1000 °C and 50 atm. For continuous diamond growth, this deposition-cleaning cycle was repeated. It was found that the diamond growth occurred only when using reactant gases containing a methyl group (CH_3—) such as methane, ethane, propane, methyl chloride, methyl mercaptane, and acetone, and that hydrocarbon gases not containing methyl groups, such as benzene, did not grow diamonds by this thermal process. However, the estimated growth rate was only about 1 Å/h, and thus the increase in the growth rate was one of the major issues to be solved in the subsequent studies. Useful conclusions obtained from Eversole's experiments are summarized as follows: First, a temperature of about 1000 °C is necessary for the diamond growth. Second, the methyl radicals generated by the dissociation of the reactant gases are needed for the diamond growth in the thermal CVD process. Finally, hydrogen at 1000 °C effectively removes the black carbon component codeposited with diamond.

On the basis of Eversole's findings, a Russian group, headed by Derjaguin, has been investigating the diamond synthesis since the 1960s using a variety of experimental methods.[8–26] These are (1) the usual thermal decomposition of hydrocarbon gases, (2) thermal decomposition using a Xe lamp,[8–10] (3) a thermal pulse method using a Xe lamp,[15] (4) the glow-discharge method,[18,22] (5) a hot-filament method,[19] (6) a chemical transport reaction (CTR) method,[21,24] and (7) a laser method.[23] Unfortunately, it is not possible to repeat the experiments as no experimental setup and conditions are described in their papers. However, the observed results on diamond formation seem to be useful and therefore are summarized below. Reviews by Fedoseev and Varnin[25] and by Fedoseev *et al.*[26] should also be consulted.

(1) *Filamentary diamonds.*[8–10] In the thermal decomposition of hydrocarbon gases, filamentary diamonds were formed on single-crystal diamond substrates (the diameters of the filaments were 10–20 μm and the maximum length was 400 μm). A possible mechanism of the filament growth is VLS (vapor-liquid-solid) due to accidental precipitation of metal particles on the substrates before the experiments.

(2) *Isotope partition.* In the thermal decomposition of hydrocarbon gases labeled with ^{13}C, the isotope was contained in the synthesized diamond more richly than in the deposited graphite.

(3) *Partial carbon pressure.*[24] Let $p_e(D)$ and $p_e(G)$ be the partial pressures of carbon in equilibrium with diamond and graphite, respectively; then an approximate relation, $p_e(D) \sim 2p_e(G) \sim 10^{-13}$ Torr, holds at temperatures between 1000 and 2000 °C. Under usual thermal CVD conditions, the carbon partial pressure p is about 10^{-7} Torr, roughly 10^6 times more supersaturated than $p_e(D)$.

(4) *Nucleation.*[12,13] Let $J(D)$ and $J(G)$ be the nucleation rates of diamond and graphite, respectively, then the ratio $J(D)/J(G)$ becomes the maximum $J(D)/J(G)=2$ at $p/p_e(G)=3.2$.

(5) *Atomic hydrogen.*[19,25,26] As observed by Eversole,[7] hydrogen gas at high temperature actively removes the black carbon co-deposited with diamond. The Russian group found that atomic hydrogen can etch graphite a few orders of magnitude faster than diamond, so that the introduction of atomic hydrogen on the substrate surface could greatly suppress the co-deposition of graphite. Atomic hydrogen in excess of the equilibrium concentration can be generated by passing hydrogen gas over a heated tungsten filament or by glow discharge. It was reported that diamond films with a thickness of a few micrometers were obtained by the hot-filament method.

(6) *Graphitic clusters.*[14,20] Graphitic carbon clusters tend to take two-dimensional planar forms, because they grow along the *ab* plane of the corresponding graphite crystal much faster than along the *c* axis.

(7) *Growth rate of the clusters.* The order of the cluster growth rates is as follows: Diamond cluster growth on diamond is faster than graphitic cluster growth on diamond, which is greater than graphitic cluster growth on graphite.

(8) *Epitaxial growth.*[18,22] In the glow-discharge method of diamond deposition on (111) surfaces of bulk diamond crystals, new diamond film grows epitaxially in the earliest stage, but when the film thickness reaches about 0.1 μm, polycrystalline diamonds with particle sizes of 50–200 Å begin to grow. After the film thickness reaches 1–2 μm, the surface becomes either polycrystalline or well-textured with [110] axes oriented perpendicular to the substrate, depending on experimental conditions.

(9) *The CTR method.*[17,24] This is the most successful technique of diamond synthesis in the Derjaguin group. Although the experimental setup is not described, it is presumably such that a solid carbon source and a substrate were placed in a radio-frequency (rf) heated reaction vessel under a hydrogen gas flow, so that chemically active hydrocarbon species, generated by chemical reactions between hydrogen and carbon, were transported over the substrate, thus producing a diamond deposit. The co-deposition of graphite was greatly reduced as it was continuously removed by atomic hydrogen excessively present in the reaction vessel. The growth rate of diamond was about 1 μm/h, much faster than in the Eversole method. When bulk single-crystal diamonds were used for substrates in the CTR method, either polycrystalline diamond films with grain sizes of 15–20 Å or single-crystalline films were formed. Spontaneous nucleation of diamonds occurred on surface defects, e.g.,

scratches, grain boundaries, and dislocations. On the other hand, when foreign materials such as Cu, Si, and W were used for substrates, only diamond particles were grown. The nucleation density of diamonds on carbide-forming substrates, e.g., Si, Mo, and W, was 1 or 2 orders of magnitude higher than the densities on non-carbide-forming substrates, e.g., Cu and Au. In the latter case, diamond particles had well-defined crystal habits of regular polyhedra with lower halves of the particles being cut by the substrate surface. From the crystal habits, the ratio of the growth rates in the [111] and [100] directions, v_{100}/v_{111}, was determined. Upon increasing the substrate temperature, the crystal habits changed from regular octahedral ($v_{100}/v_{111} > 3$) to cubic ($v_{100}/v_{111} < 1/\sqrt{3}$) via intermediate cubo-octahedrals as shown in Fig. 1. Diamond particles with twin structures were also observed. Furthermore, p-type semiconductive diamond films were deposited on bulk diamonds by introducing a small amount of boron-containing gas in the reaction vessel. The activation energy for the electric conduction in the films changed from 0.37 to 0.1 eV as the doping concentration was increased from 10^{17} to 10^{19} cm^{-3}. For other works not described here, readers should see Refs. 27–30.

On the basis of these data and other information, as well as their own research over a decade about the synthesis of diamond from gas phase, Setaka and co-workers[1,31–36] found three different CVD methods for diamond synthesis using hot-filament, rf-wave, and microwave methods as shown in Figs. 2(a)–2(c). The most crucial aspect of their findings is that in order to obtain almost pure, crystalline diamonds, the hydrocarbon gas, e.g., methane, used in the synthesis has to be diluted by hydrogen to as low as about 1%. With the use of these methods, diamonds were deposited on various substrates such as Si, SiC, WC, Si_3N_4, Al_2O_3, Ta, Mo, and W at a rate of 0.3–0.5 μm/h.

Figure 2(a) schematically shows the apparatus of the

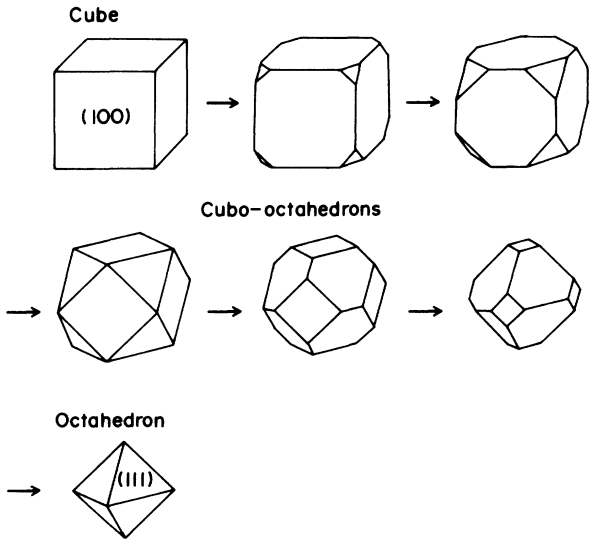

FIG. 1. Polyhedrals of diamond.

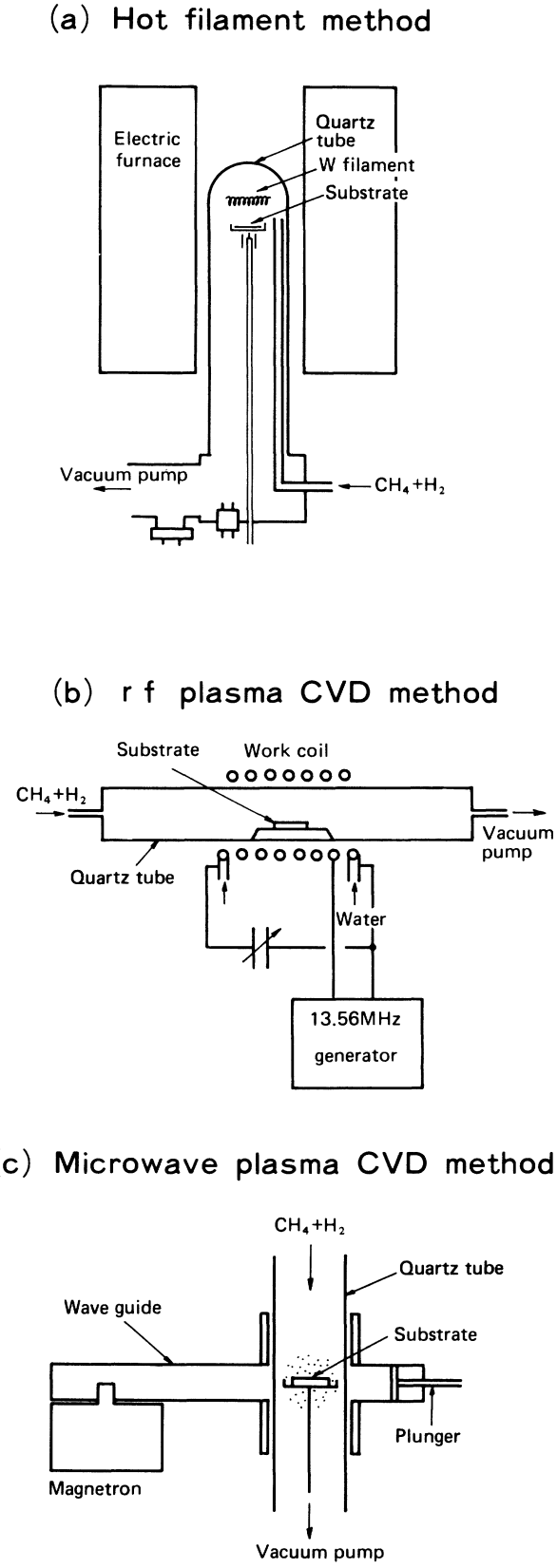

FIG. 2. CVD methods for diamond synthesis proposed by Setaka and co-workers (Refs. 1 and 31–36): (a) hot-filament method, (b) rf plasma CVD method, and (c) microwave plasma CVD method, which is used in the present article.

hot-filament method.[32–34] A tungsten filament is placed about 10 mm above the substrate and electrically heated to about 2000 °C. The quartz-tube reaction chamber is placed in an electric furnace and heated to about 600 °C. Because of the thermal radiation from the filament and the furnace, the temperature at the substrate surface reaches more than 1000 °C, and surface processes such as molecular dissociation, diffusion, and chemical reactions are activated. More importantly, the hot filament generates atomic hydrogen and chemically active fragmentary hydrocarbons (ions and radicals) by dissociating molecular hydrogen and methane, respectively. These chemically active species have unexpectedly long lifetimes and can travel to the substrate surface, causing spontaneous growth of diamonds.

Diamonds can also grow on substrates immersed in a hydrocarbon-hydrogen mixed-gas plasma generated by an irradiation of rf waves[36] or microwaves,[35] as shown in Figs. 2(b) and 2(c). In the microwave method [see Fig. 2(c)], which is used in the present paper, a substrate is placed in a quartz tube which penetrates perpendicularly to a rectangular wave guide, and microwaves of 2.45 GHz (the frequency allowed for industrial use), generated by a magnetron, are guided to the quartz tube, producing a plasma. The position of the plunger is adjusted so that the substrate is entirely immersed in the plasma. In both hot-filament and plasma CVD methods, the gas pressure in the reaction chamber is about 40 Torr and the gas flow rate is 10–100 sccm (standard cubic centimeters per minute).

If a commercially available mirror-polished Si wafer is used for the substrate, only diamond particles are grown, as seen in Fig. 3. Setaka *et al.*, however, found that if the Si wafer was polished with diamond powder of a few micrometer size, the nucleation density was markedly increased, and as a result, polycrystalline diamond films are formed, as seen in Fig. 4. It is therefore inferred that the surface defects produced on the wafer surface by polishing provide active sites for diamond nucleations.

The mechanism of diamond formation is not fully understood yet, but Setaka[37] proposed a conceptual diagram

FIG. 3. Diamond particles grown on si substrate.

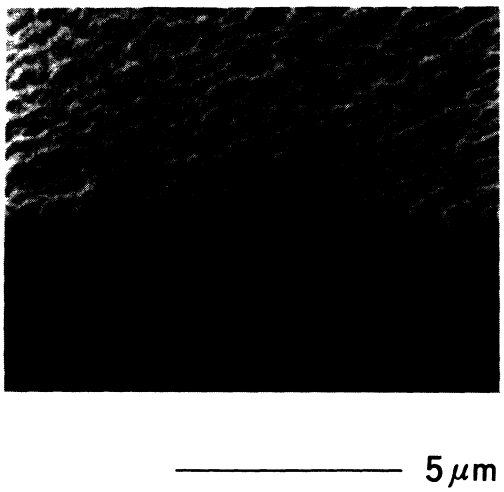

FIG. 4. A broken edge of a polycrystalline diamond film grown on a Si substrate at the CH_4 concentration $c = 1$ vol % for 7 h. Note that the film exhibits a columnar growth.

for diamond formation as shown in Fig. 5 for the case of the microwave method. Here, methane and hydrogen are dissociated in the plasma, and chemically active fragmentary hydrocarbon ions and radicals, as well as atomic hydrogen, are generated. The hydrocarbon species spontaneously diffuse and are adsorbed on the substrate. In the earliest stage of the synthesis, when the substrate is not covered with diamonds, carbon clusters are formed

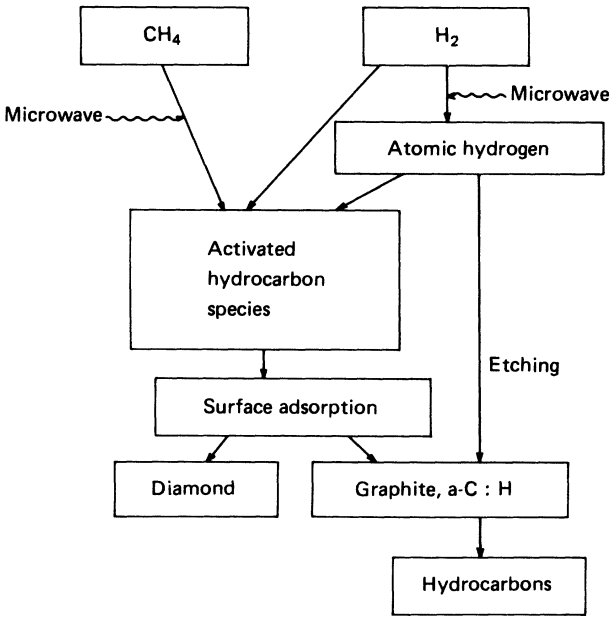

FIG. 5. A mechanism of diamond formation proposed by Setaka (Ref. 37).

on the substrate surface, as a result of numerous chemical reactions releasing hydrogen. The majority of the clusters have thermodynamically stable graphitic and amorphous structures, but metastable diamond structures are also formed due to thermodynamic fluctuation. Since the chemical reaction rate of graphite with atomic hydrogen is about 20 to 30 times faster than that of diamond, graphitic carbon clusters are removed rapidly from the substrate surface, and as a result, only clusters with diamond structure stay and grow. Furthermore, atomic hydrogen attacks unsaturated sp^1 and sp^2 bonds between carbon atoms in the clusters to convert them into the tetrahedral sp^3 bonds. Thus, atomic hydrogen facilitates the formation of diamond clusters with only sp^3 bonds, suppressing other forms of clusters having unsaturated bonds.

The growth mechanism of diamond clusters is perhaps purely chemical. It is supposed that chemically active species such as methyl radicals arriving at the surface release hydrogen to form C—C covalent bonds with the carbon atoms of the cluster. Thus, the surfaces of CVD diamonds are terminated by C—H bonds. For detailed theoretical investigations on microscopic processes of epitaxial diamond growth at the (111) diamond surface, see work by Tsuda *et al.*[38,39]

For the source gas in the diamond synthesis, usually a mixture of CH_4 and H_2 is used. Other hydrocarbon gases such as ethane, ethylene and acetylene can be used in the microwave plasma CVD method. This is in strong contrast to the thermal CVD and hot-filament methods, in which only CH_3-containing gases can grow diamonds. Hirose and his co-workers,[40] however, found using the hot-filament method at pressures below atmospheric that organic compounds such as acetone (CH_3—CO—CH_3), ethanol (CH_3CH_2OH) and many other organic compounds, including CH_3— groups and O atoms, can grow diamonds at a rate of 8 μm/h, about 20 times faster than when CH_4 is used. The marked increase in the growth rate is attributed to the high density of methyl radicals in the plasma and the presence of hydroxyl radicals (—OH) which can etch graphite very rapidly.

Concluding this review, it is suggested that the reader should consult Refs. 41 and 42 for the electron-assisted chemical-vapor-deposition (EACVD) method, Refs. 43 and 44 for plasma diagnostic, and Refs. 45 and 46 for the microwave plasma CVD.

A unique characteristic of the diamonds synthesized by CVD is that they have well-defined crystal habits, which strongly depend on experimental conditions. Thus, as a first step toward fully understanding the properties of diamond films, an investigation is made in this paper of the morphology and growth of the diamond films deposited on Si from a microwave-generated plasma of methane-hydrogen mixed gas. The characterization of the films is made using scanning electron microscopy (SEM), x-ray diffraction, reflection high-energy electron diffraction (RHEED), Raman scattering, and infrared absorption. In the next section, experimental setup and procedure are described. Section III presents the results of film morphology and characterization. The SEM results on the film growth are presented in Sec. IV. Finally, a discussion is given in Sec. V.

II. EXPERIMENT

The setup of the experimental apparatus, schematically depicted in Fig. 6, is similar to that established by Kamo *et al.*[35] [see Fig. 2(c)] except that the quartz-tube reaction chamber is placed horizontally. The 2.45-GHz microwave used is guided through an isolator and a three-stub tuner to the quartz tube chamber of 44 mm i.d., which penetrates perpendicularly through the rectangular wave guide. A plunger is attached to the end of the waveguide.

A Si substrate, 2×1 cm^2 in area and 0.5 mm thick, was placed in the middle of the quartz-tube–waveguide intersection and held vertically by a quartz holder with a substrate face directed toward a viewing port. The substrate temperature was measured by an optical thermometer, monitoring the 900-nm emission. Since the emissivity of the substrate during the synthesis is not known, the blackbody radiation was assumed for temperature estimation, and no correction was made for the absorption due to the quartz viewing port. Therefore, "temperature" as used in this paper simply denotes the indicator output of the thermometer and does not represent the real temperature. In all experiments described here, the substrate temperature was kept at 800 °C, and it is assumed that the real temperature was somewhat higher than this for the reasons stated above. The effect of the radiation from the plasma was negligibly small. For the source gas, H_2 and a mixture of 5 vol % CH_4 and 95 vol % H_2 gases were used. These were mixed at a desired concentration using mass-flow controllers. The gas pressure was monitored by a diaphragm-type pressure sensor.

The start-up procedure of the experiment is as follows: After the substrate was positioned, the reaction chamber was evacuated to a minimum pressure with a main valve fully opened. The reaction gas was then introduced into the chamber at a rate of 100 sccm with the main valve now closed, and the microwave radiation of 400 W was supplied at the same time. The plasma was spontaneously turned on when the gas pressure reached a few Torr. The gas pressure was finally adjusted and maintained at

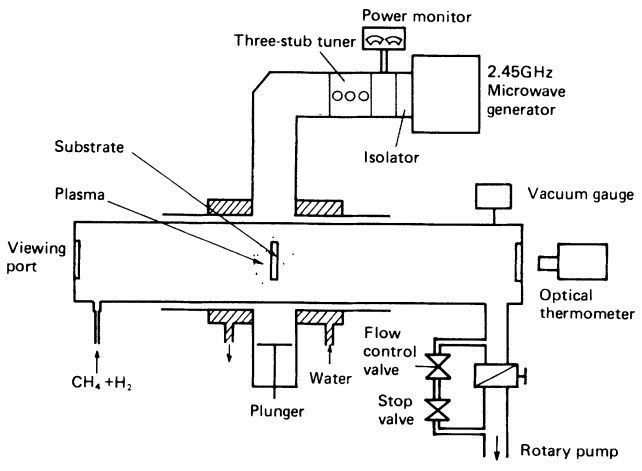

FIG. 6. Microwave plasma CVD system.

30 Torr using a flow control valve. The microwave power was then reduced to 300–350 W to keep the substrate temperature at 800 °C. The position of the plasma was adjusted by the plunger so that the substrate was entirely immersed in the plasma. Finally, the reflected microwave power was minimized to less than 10 W by the three-stub tuner. Under these experimental conditions, the plasma did not touch the quartz wall. The substrate temperature depends strongly on the microwave power and gas pressure, and less strongly on the gas flow rate, as the microwave induction heating and the plasma-gas collision are responsible for the substrate heating.

As stated in the preceding section, the nucleation density of diamond is greatly increased by polishing substrates with a diamond powder. In the present experiment, Si wafers were polished with a diamond paste of $\frac{1}{4}$ μm size for 1 h, cut to size, washed by distilled water, alcohol, and acetone using an ultrasonic cleaner, and finally dried in the air. It is using such substrates that polycrystalline diamond films were grown, as shown in Fig. 4.

When the film growth was studied, the polished substrates were annealed at 800 °C for 3–5 min in a H_2 plasma before the diamond synthesis in order to decrease the nucleation density. Otherwise, diamond films were formed only within 1 h and the detailed crystal habits of the diamond particles could not be observed by SEM as they were too small.

The syntheses were usually carried out for 7 h in the investigation of the surface morphology. On the other hand, in the investigation of the film growth, the synthesis was interrupted every few hours for SEM observation, and the specimen was returned to the chamber for further growth.

It should be noted that there exists a nonuniformity of the morphology across the substrate: Generally, the grain sizes along the long edge of the substrate were much larger than those in the central part. Moreover, well-defined crystal habits were present along the long edges even at such a high CH_4 concentration as 2.0 vol % (all subsequent concentrations c are in vol %), in which case only a microcrystalline structure was observed in the central part of the specimen. Thus, for the study of the film morphology in Sec. III, SEM pictures of only the center of the specimen are presented. On the other hand, for the study of the film growth in Sec. IV, SEM pictures of either the center or near the edge of the specimen are shown.

III. MORPHOLOGY OF THE FILM SURFACES

This section presents the morphology of the diamond films deposited for 7 h on Si(100) substrates at different CH_4 concentrations (hereafter denoted by c) below 2%. Properties of the films were analyzed using x-ray diffraction, RHEED, Raman scattering, and infrared absorption. Figure 4 shows a side view of a film deposited on a Si(100) substrate at $c=1.0\%$. It is clearly seen that the film undergoes a columnar growth. Figure 7 plots the film thickness as a function of the CH_4 concentration.

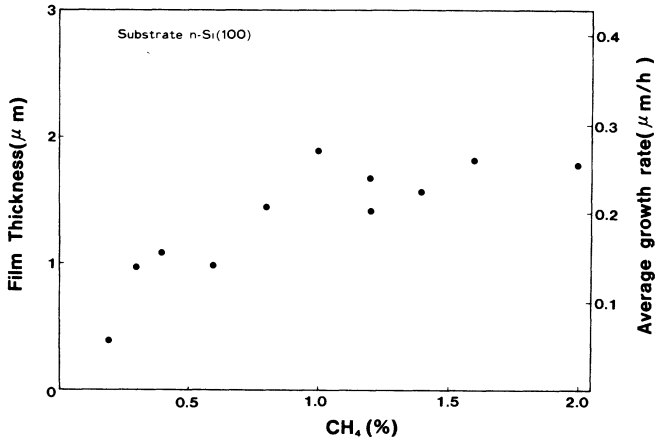

FIG. 7. Film thicknesses after 7 h of the CVD synthesis. The substrates used are Si(100).

The thickness increases rapidly with c up to $c=0.6\%$ and then increases only slowly to about 1.5 μm at higher concentrations. It should be noted that at $c=0.2\%$, only diamond particles are formed on the substrate, as seen later in Fig. 8(a), so that the thickness in this case means the average height of the particles. In Fig. 7, the "growth rate" on the right ordinate stands for the film thickness divided by the synthesis time, 7 h. Since the growth rate during the nucleation stage is low, it is expected that if the synthesis was carried out longer than 7 h, the growth rate would be larger. In fact, the growth rate after 60 h of synthesis at $c=1.2\%$ is 0.35 μm/h, about 40% larger than the value shown in Fig. 7. It should be emphasized that given the wide range of morphology structures and the existence of the nucleation stage, the film thickness and the growth rate shown here are at best semiquantitative.

Figures 8(a)–8(i) show the SEM pictures of the film surfaces. At $c=0.2\%$ [see Fig. 8(a)], only particles are obtained which have various cubo-octahedral shapes as shown in Fig. 1. At $c=0.3\%$ [see Fig. 8(b)], the film thickness is only about 0.9 μm (see Fig. 7) and the substrate is thinly covered with diamond particles having triangular (111) crystallographic planes. Most particles are not single crystals but have twin structures as described in Ref. 32. The surface morphology changes markedly at $c=0.4\%$ [see Fig. 8(c)], where the majority of the crystallographic planes appearing on the film surface are (100), characteristic of the planar square surfaces, overlapped by the secondary growth of diamonds. At $c=0.6\%$ [see Fig. 8(d)], the film surface consists of (100) faces only, and there are considerable distributions for the areas and directions of (100) faces.

The (100) features become more prominent as c increases to 1.0% [see Figs. 8(e) and 8(f)]. It should be noted here that the square (100) face does not correspond to one of the faces of a diamond cube as shown in Fig. 1, because the sides of the (100) face are very rough and no well-defined crystallographic planes of diamond are observed. This means that (100) faces undergo an anisotropic growth, almost perpendicularly to the Si substrate

plane. However, (100) faces are not directed exactly normal to the substrate plane but there is a certain distribution of the direction angles within roughly 30° about the substrate normal. Although it is not apparent in Figs. 8(e) and 8(f), there exist small grains with well-defined crystallographic planes [perhaps (100)] behind the prominent (100) faces. Therefore, it is presumed that the prominent (100) faces are the result of growth competition between the grains. Notice also that some of the (100) faces are overlapping the others as a consequence of the interference during the growth. It has been reported[47] that when two grains undergoing a columnar growth are intersecting, the one which is more perpendicular to the substrate plane takes over the other. If this is the case for the diamond films, the (100) faces appearing on the film surface would be more parallel to the film surface as the synthesis proceeds. Indeed, there is an indication observed by Setaka *et al.* that this actually happens.[48]

As the concentration increases beyond $c = 1\%$, the density of (100) faces decreases and the square feature

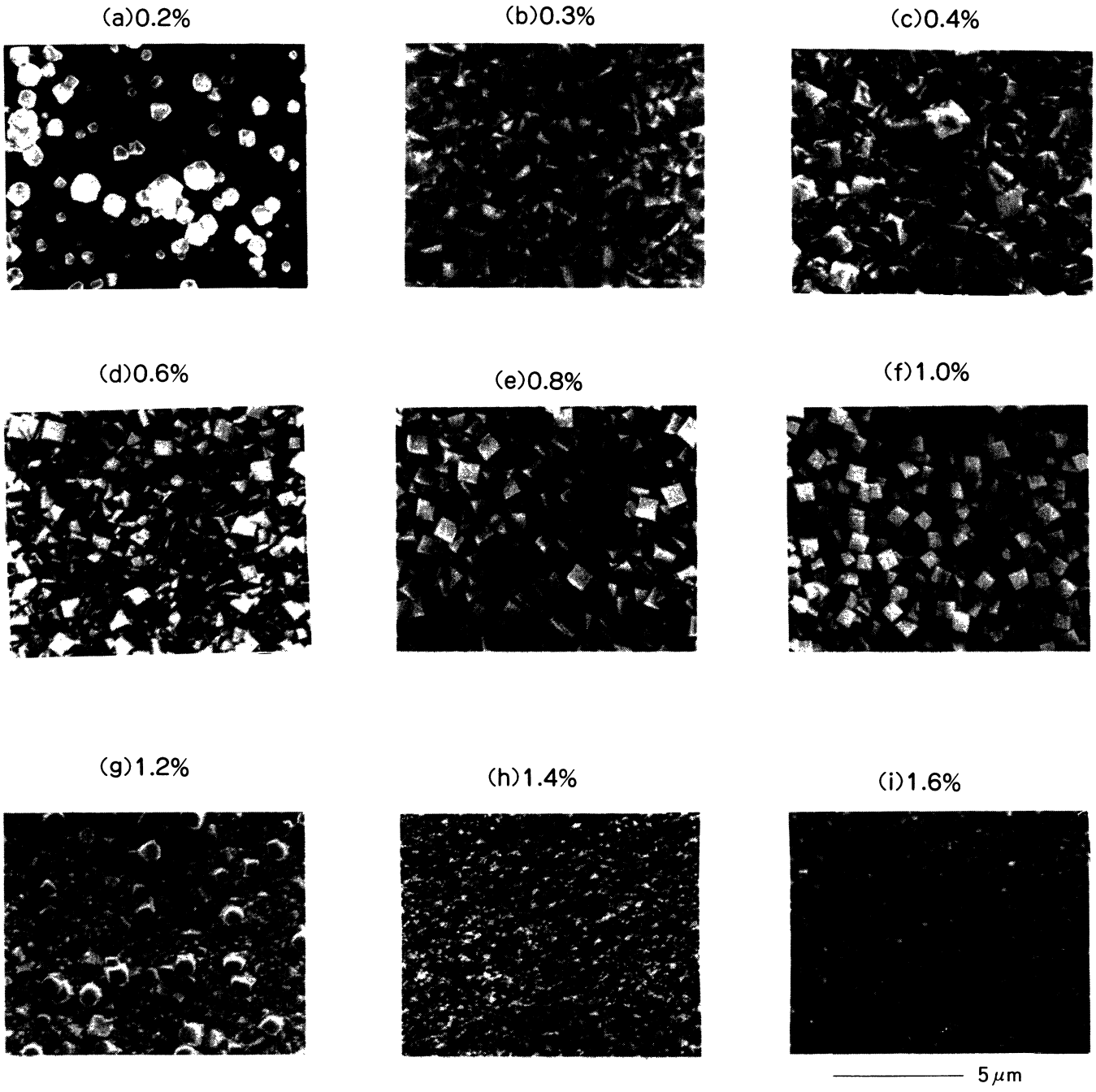

FIG. 8. Surface morphology of the diamond films observed by SEM: (a) 0.2%, (b) 0.3%, (c) 0.4%, (d) 0.6%, (e) 0.8%, (f) 1.0%, (g) 1.2%, (h) 1.4%, and (i) 1.6%. The films are deposited on Si(100) for 7 h.

gradually fades as seen in Fig. 8(g). It is noted that there are considerable fluctuations in the surface morphology for each run. For instance, in some specimens synthesized for $c=1.2\%$, the film surfaces have well-defined (100) faces like the one shown in Fig. 8(f), but in other runs, they have a morphology as shown in Fig. 8(g). A primary cause for the fluctuation is perhaps that the substrate could not be placed at exactly the same position with respect to the plasma in each experiment. The inhomogeneity of temperature over the substrate seems to have only a minor effect on the fluctuation, because the substrate temperature is quite uniform except for the edges of the substrate. For concentrations higher than $c \simeq 1.4\%$, the film surfaces become totally microcrystalline and no crystallographic planes of diamond are observed within the resolution of the SEM used. Although the film surfaces at $c=1.4\%$ [see Fig. 8(h)] and 1.6% [see Fig. 8(i)] are both microcrystalline, the surface of Fig. 8(i) has a so-called "cauliflower" structure already reported in films of other materials such as graphite.[47]

Similar experiments were repeated using Si(111) substrates, and basically the same results were obtained. Thus, the present results can be summarized as in Fig. 9. The fact that the surface morphology changes from (111) to (100) in a very narrow range of the CH_4 concentration around $c=0.4\%$ indicates how critically the morphology depends on c, and presumably also on other thermodynamic conditions of the plasma. This is in strong contrast to the fact that the microcrystallization of the film takes place over a relatively wide concentration range above 1.2%.

X-ray diffraction measurements were carried out for the films synthesized. Table I lists the observed result for the film synthesized at $c=1.0\%$, which indicates that the lattice spacings of the CVD diamonds have the same values as those of natural diamond within experimental error. Figure 10 shows the x-ray spectra of the films synthesized for different c. At low CH_4 concentrations, the intensities of x-ray diffraction lines are similar to the standard pattern of diamond powder. As the CH_4 concentration increases, the intensity of the (111) line at $2\theta=43.9°$ decreases, whereas the intensity of the (220) line at $2\theta=75.4°$ remains almost the same. This fact implies, first, that the diamond component in the film decreases with c, and second, that the orientations of the diamond grains are almost random at low CH_4 concentrations, whereas (110) crystallographic planes of diamond tend to be more parallel to the substrate surface at higher concentrations. The diffraction intensity of (400) at $2\theta=119.6°$ is extremely weak at low c, but becomes detectable around $c=1\%$ in accordance with the unidirectionally ordered orientations of (100) faces. No discrete change in the x-ray intensities is observed at $c=0.4\%$ in spite of the discrete change in the surface morphology.

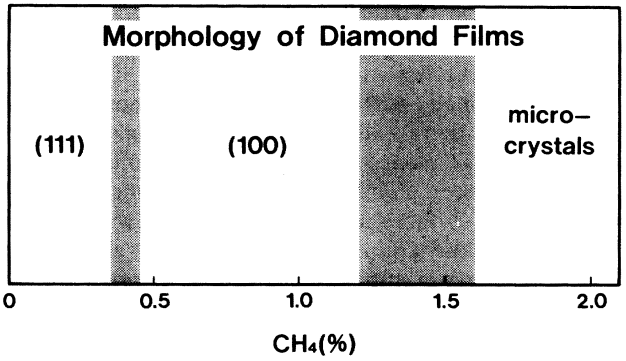

FIG. 9. Morphology of the diamond films with respect to the CH_4 concentration.

Figure 11 shows a RHEED pattern of the film synthesized for 7 h on a Si(111) substrate at $c=1.0\%$. The lattice spacings deduced are also listed in Table I, which, like the x-ray data, are in good agreement with the American Society for Testing Materials (ASTM) values. Figure 11 is characterized by intense spot patterns for (111), (220), and (311) diffractions, indicating that fairly large grains are contained in the film. Such spot patterns are observed from about half of the specimens and the rest have ring-type diffraction patterns, consisting of small spots only. The diffraction of (400) is very weak despite the fact that (100) faces of diamonds appear on the film surface, as seen in Fig. 8(f). This is presumably because the (100) faces are not oriented exactly normal to the film surface but somewhat tilted, as discussed before. From the selection rule of the first-order diffraction, the (222) diffraction is not allowed. However, such diffractions

TABLE I. Interplanar spacings (in units of Å) of diamonds synthesized at $c=1.0\%$ for 7 h.

	ASTM		Diamond films	
hkl	*d*	Intensity	X ray[a]	RHEED[a]
111	2.06	100	2.058 *S*	2.089 *S*
220	1.261	25	1.260 *M*	1.265 *S*
311	1.0754	16	1.074 *M*	1.079 *S*
222	(1.030)[b]			1.038 *W*
400	0.8916	8	0.891 *W*	0.893 *M*
331	0.8182	16		0.813 *W*

[a]*S*, *M*, and *W* stand for relative intensities: *S* strong; *M* medium; and *W* weak.
[b]This line is not allowed by the first-order selection rules.

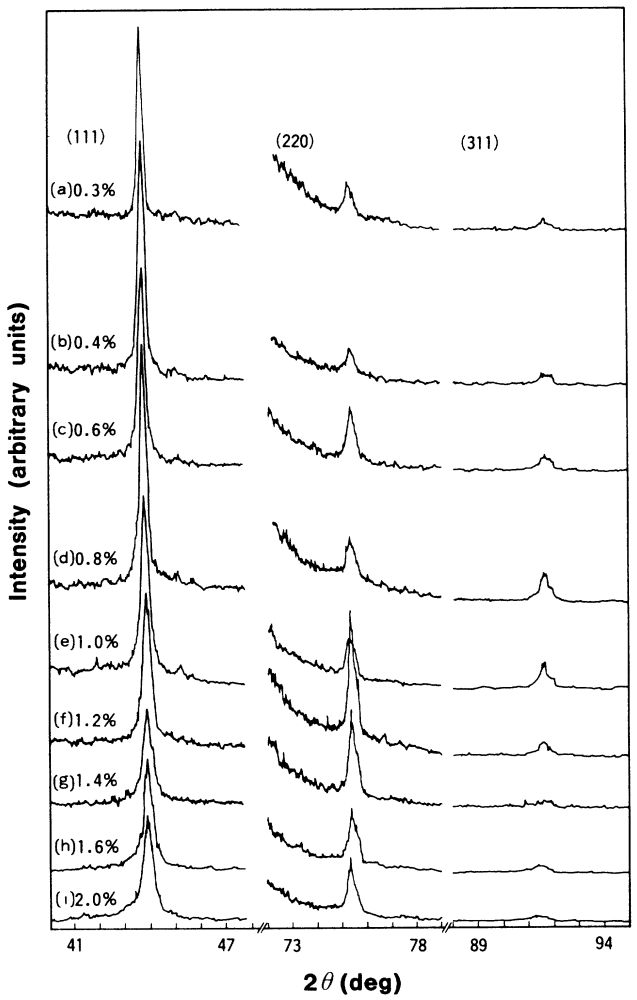

FIG. 10. X-ray diffraction spectra of diamond films deposited on Si(100) substrates at different CH_4 concentrations: (a) 0.3%, (b) 0.4%, (c) 0.6%, (d) 0.8%, (e) 1.0%, (f) 1.2%, (g) 1.4%, (h) 1.6%, and (i) 2.0%. A weak diffraction of (400) is seen at 119.6° for $c = 1.0\%$ and 1.2%.

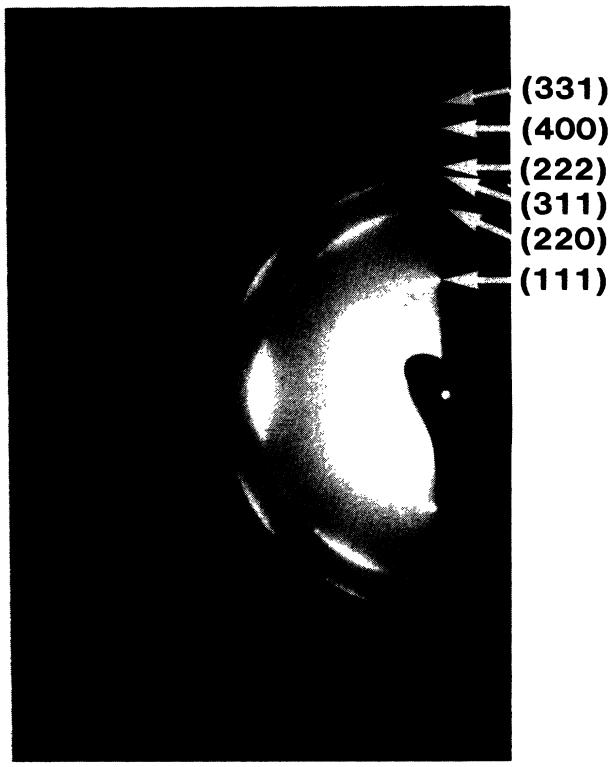

FIG. 11. RHEED pattern of a diamond film deposited on a Si(111) substrate at $c = 1.0\%$ for 7 h. The lattice spacings evaluated from the pattern are listed in Table I.

have been reported in Refs. 35 and 40, and are attributed to higher-order diffractions which can appear in the specimens that have a good crystallinity. No discrete change in the diffraction pattern was observed around $c = 0.4\%$ and $c = 1.2\%$.

Figure 12 depicts the Raman spectra of the diamond films. The assignments of the bands are as follows:[49–52] a sharp line at 1334 cm^{-1} arises from diamond, while a broad band around 1500 cm^{-1} arises from graphite and other forms of carbon including amorphous. Although not prominent in all the spectra, a weak, broad band exists at about 1350 cm^{-1}, overlapping the diamond line. This feature is attributed to a disordered structure or to reduced grain sizes of graphite. This size effect has been discussed in great detail in Ref. 53. Finally, a weak band at 1140 cm^{-1} is assigned to C—C and C=C stretching modes of polyenelike molecules.[54,55]

As seen in Fig. 12, the intensity of the 1500-cm^{-1} band increases relative to the 1334-cm^{-1} band with c. This result demonstrates that the concentration of nondiamond components in the film increases as the CH_4 concentration increases. It should, however, be noted that the ratio of the intensities of the two Raman bands is not proportional to the ratio of diamond to nondiamond concentrations because the magnitude of the Raman scattering tensor is 30 times larger for graphite and a-C than for diamond.[49] Therefore, even though the 1332-cm^{-1} intensity is weaker than the 1550-cm^{-1} intensity, as seen in Fig. 12(f), for instance, the actual diamond-to-nondiamond concentration ratio is much higher than the 1332/1550 intensity ratio. This is consistent with the x-ray and electron diffraction results that the diamond diffraction pattern is still observed even for $c = 2\%$. Like other data, no discrete change in the spectra is found at $c = 0.4\%$ or around $c = 1.2\%$ where the film morphology changes markedly.

Infrared absorption spectra in the C—H vibrational region were measured. However, as seen in Fig. 13(a), the absorption intensity of the films synthesized for 7 h are so weak that no systematic trend with c was found. The spectra of thicker films, synthesized for 97 h at $c = 0.3\%$ and for 52 h at $c = 1.2\%$, shown in Figs. 13(b) and 13(c), respectively, have stronger absorption intensities, and the detailed feature of the spectra are now detected.[56,57] The

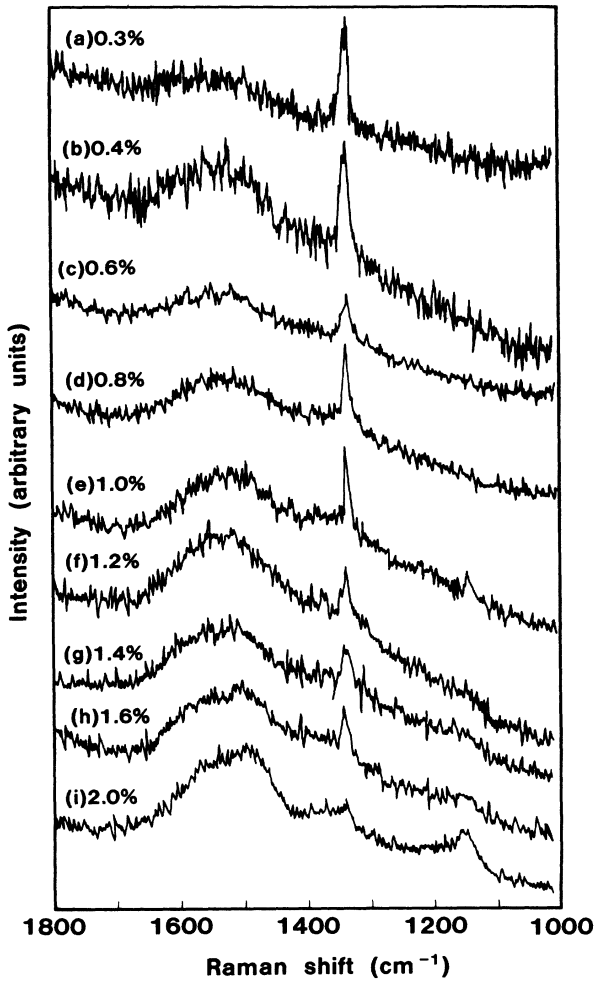

FIG. 12. Raman spectra of diamond films deposited on Si(100) substrates for 7 h. For bulk diamond, only a single, sharp line is observed at 1332 cm^{-1}.

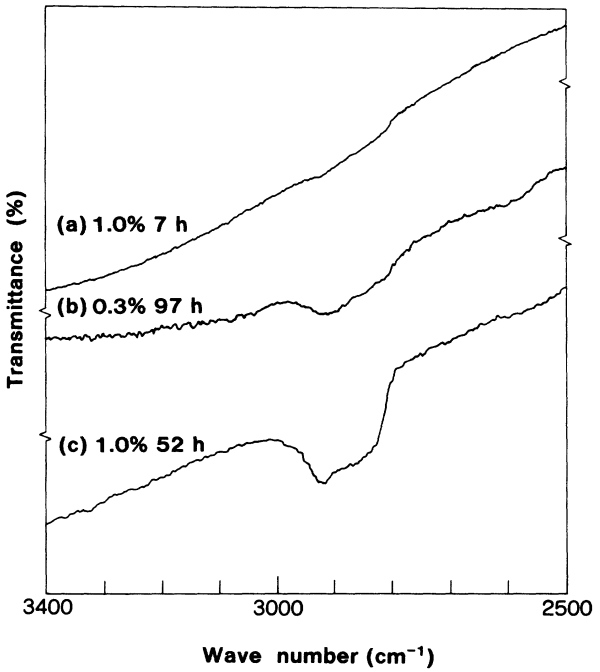

FIG. 13. Infrared absorption spectra of diamond films in the C-H vibrational region: (a) $c=1.0\%$, synthesized for 7 h, (b) $c=0.3\%$ for 97 h, and (c) $c=1.0\%$ for 52 h.

infrared bands have a main peak at 2920 cm^{-1} and a broad band around 2850 cm^{-1}. The former arises from CH and CH_2 vibrations where the C atoms have sp^3 bonds with adjacent C atoms, whereas the latter arises from CH_2 vibrations where the C atoms also have sp^3 bonds. A rough estimate based on Ref. 58 shows that the specimens of Fig. 13(b) and 13(c) contain only 3–4 at. % of hydrogen. The hydrogen content in the diamond films is much smaller than in a-C:H films, which usually contain more than 10% of hydrogen, because the substrate temperature for the diamond deposition in the present work was maintained at a temperature as high as 800 °C during the synthesis. It is argued by Setaka *et al.* that the hydrogen is chemisorbed only at the film surface and grain boundaries, and not contained in the diamond grains.[59]

Briefly summarizing the results presented in this section, it is found that the film morphology changes from (111) to (100) at $c=0.4\%$ and from (100) to microcrystalline at $c=1.2$–1.6%, as seen in Fig. 9. X-ray and Raman data show that as c increases the diamond concentration decreases, whereas graphitic and a-C components increase. The observed data exhibit continuous changes with c in spite of the discrete changes in the surface morphology at $c=0.4\%$ and above $c=1.2\%$.

IV. GROWTH OF DIAMOND FILMS

The purpose of this section is to investigate how the surface structures observed in the previous section are formed in the course of the diamond synthesis. To this end, the following method was used: The CVD synthesis was interrupted every few hours and the specimen was taken out of the reaction chamber to examine exactly the same position on the film surface by SEM. Among several runs undertaken for different experimental conditions, the results of $c=0.3\%$, 0.8%, and 1.2% are presented below. It may be noticed that the morphology observed in the present method is possibly influenced by the following nonintrinsic effects: first, the specimens were exposed to 800 °C during the synthesis and to room-temperature in the SEM observation so that they were subject to a significantly large thermal hysteresis. Secondly, every time the samples were taken out of the chamber, they were exposed to the air, resulting in an adsorption of gases. Since there is no good reference to compare in order to see these effects, it is difficult to investigate them any further. However, the experimental results showed no such extrinsic effect on the morphology. Nevertheless, it should be kept in mind that the present results were obtained under these conditions.

As already described in Sec. II, the Si substrates used in this section were polished by a diamond paste and furthermore, they were immersed in the H_2 plasma for about 5 min at 800 °C before the syntheses in order to de-

crease the nucleation density. This pretreatment is needed, because otherwise the crystal habits of the diamond particles, which were formed in the early stage of the synthesis, cannot be observed clearly within the SEM resolution.

Figures 14(a)–14(c) show an overview of the growth process for $c=0.5\%$. The dark portion in the center of each picture is a cleaved area on the Si substrate surface made by a diamond pen before the deposition. In the earliest stage [see Fig. 14(a)], diamond particles are grown on the substrate surface polished by the diamond paste. In contrast, there is no nucleation on the cleaved Si area. As the synthesis goes on, the diamond particles become bigger, covering the entire Si surface except the cleaved area [see Fig. 14(b)], and then the film thickness begins to increase [see Fig. 14(c)]. It is known that diamond nucleation density on mirror-polished Si substrates is small,[31–37] as described in Sec. I. Figures 14(a)–14(c) show that it is also the case for the cleaved Si surface. However, it is still a controversy from where and how diamond nucleations start on the substrates.

Figures 15(a)–15(f) show an evolution of the diamond film surface during the synthesis at $c=0.3\%$. The location of the pictures is close to the long edge of the sample, where the grain sizes are much larger than in the center. Initially, the diamond particles have cubo-octahedral shapes [see Fig. 15(a)], and some particles have twin structures. Then the particles increase their sizes almost uniformly [see Fig. 15(b)]. Notice that there is a one-to-one correspondence between the particles of Figs. 15(a) and 15(b), and that no nucleation newly starts on the substrate surface. This implies that at this stage, surface diffusion is responsible for the growth of diamond particles. As seen in Fig. 15(c), the substrate surface is then covered entirely by the particles, and the film surface consists of (111) and (100) diamond faces, originally possessed by the discrete particles. Subsequently, the areas of the well-defined faces become larger, and at the same time, step structures become visible on the (100) faces [see Fig. 15(d)]. They are more prominent in Figs. 15(e) and 15(f). In contrast, no growth structure is seen on the (111) faces, and unlike the (100) faces, it appears that (111) faces are not flat, as seen in Figs. 15(e) and 15(f). Thus, it is possible that the growth mechanism of (111) faces could be different than that of (100). Further investigation of the (111) faces would be necessary to reveal the growth pattern using a high resolution SEM. The synthesis was continued to 97 h and basically the same features as shown in Fig. 15(f) persisted, although the surface structure was significantly modified due to the evolution of the surface morphology.

Figures 16(a)–16(e) show the growth process in the center of the specimen for $c=0.8\%$. In Fig. 16(a), a formation of diamond particles is seen. The rough substrate surface on the lower-left corner is part of a scratch mark, and no diamond is seen on it. The particles then increase their sizes, as shown in Fig. 16(b), where only (100) faces are clearly seen, and other faces, perhaps (111), are covered entirely by small grains. This indicates that in the CH_4 concentration the growth rate of (111) faces is so high that they are no longer stable. After the substrate is covered with diamonds, a secondary growth takes place between the particles [see Fig. 16(c)]. It is of interest that the (100) faces tend not to be covered by the secondary grains. After 27 h [see Fig. 16(d)], all grains have well-defined (100) faces. Note that the location of Fig. 16(d) is slightly shifted to the left from the location in the previous figures: the large (100) faces in the upper left and upper middle of Fig. 16(d) correspond to the (100) faces in the upper middle and upper right of Fig. 16(c), respec-

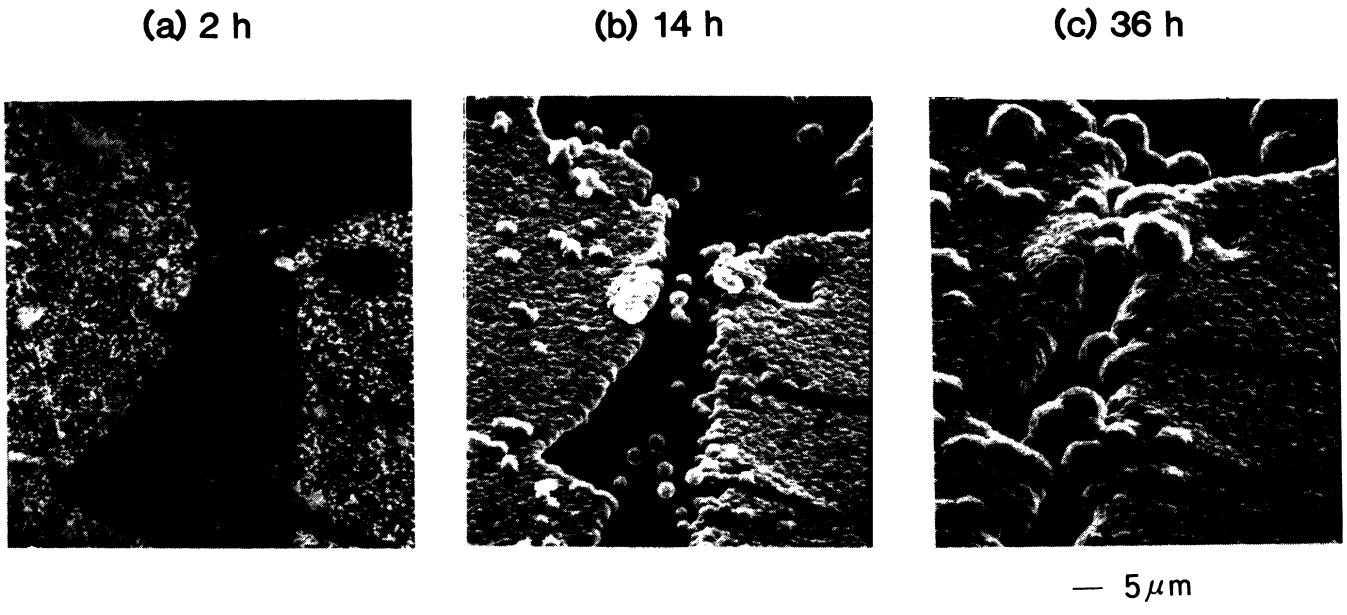

FIG. 14. Overview of a formation process of diamond film: (a) after 3 h, (b) after 12 h, and (c) after 30 h. The substrate is Si polished with a diamond paste. The dark area in the center is a scratch mark given on the substrate before the synthesis, and it is seen that the nucleation density of diamond particles is very low on the fresh Si surface.

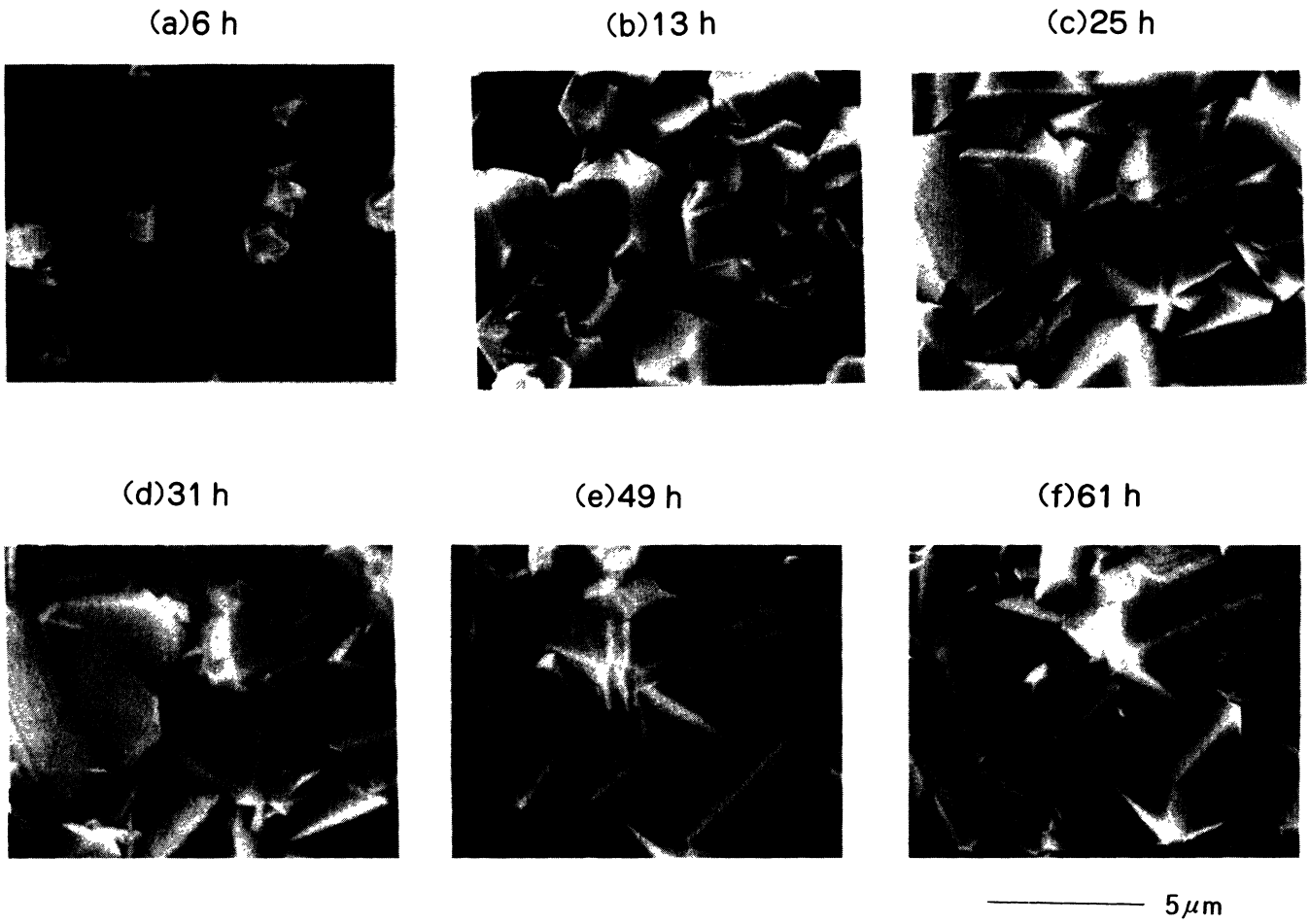

FIG. 15. Growth process for $c=0.3\%$: (a) after 6 h, (b) after 13 h, (c) after 25 h, (d) after 31 h, (e) after 49 h, and (f) after 61 h.

tively. After 31 h [see Fig. 16(e)], the surface structure changes markedly, and the areas of the diamond faces become larger. This run was continued to 53.5 h and basically the similar features as observed in Fig. 16(e) persisted.

The most important and conclusive results on the film growth were obtained for $c=1.2\%$ as shown in Figs. 17(a)–17(k). In this case, the location of the photographs is in the center of the specimen. After 3 h [see Fig. 17(a)], the substrate is already covered with small grains which have square (100) faces. Also, small crystallites are seen in the background. In the next step, after 8.3 h [see Fig. 17(b)], a secondary growth takes place and the (100) faces are being covered with small crystallites. At the same time, the (100) faces become larger. After 11.3 h [see Fig. 17(c)], the small crystallites have disappeared almost completely and the surface is covered with (100) faces of different sizes. This feature persists through 17.3 h [see Fig. 17(d)] to 26.3 h [see Fig. 17(e)]. Then a tertiary growth begins in between the (100) faces [see Fig. 17(f)] and again the film surface is covered with small crystallites [see Fig. 17(g)]. However, the tertiary crystallites have disappeared completely in Fig. 17(h), and again the film surface consists of well-defined (100) features only. In order to confirm the cyclic behavior of the higher-order growths followed by the conversion to the (100) structure, the synthesis was continued further. As expected, a fourth-order growth takes place at 50.8 h [see Fig. 17(i)], which is followed by a restructured surface [see Fig. 17(j)]. A further growth initiates at 59.8 h [see Fig. 17(k)]. The above observation clearly demonstrates that the diamond films grow cyclically through the microcrystal formation due to the higher-order growth followed by the formation of well-defined diamond faces. A similar cyclical behavior has also been observed in the growth morphology for $c=0.3\%$ and 0.8%, as seen in Figs. 15 and 16, but the changes are less clear, partly because the periods of this growth cycle are longer than for $c=1.2\%$.

Figures 18(a) and 18(b) show SEM pictures taken before and after 3.2 h of time lapse, respectively. The CH_4 concentration is 0.6%. In the central part of Fig. 18(a), there are small grains, which have disappeared in Fig. 18(b) and instead, three relatively large grains have been formed. It looks as if the small grains have "fused" with each other to form larger grains. Such changes are also

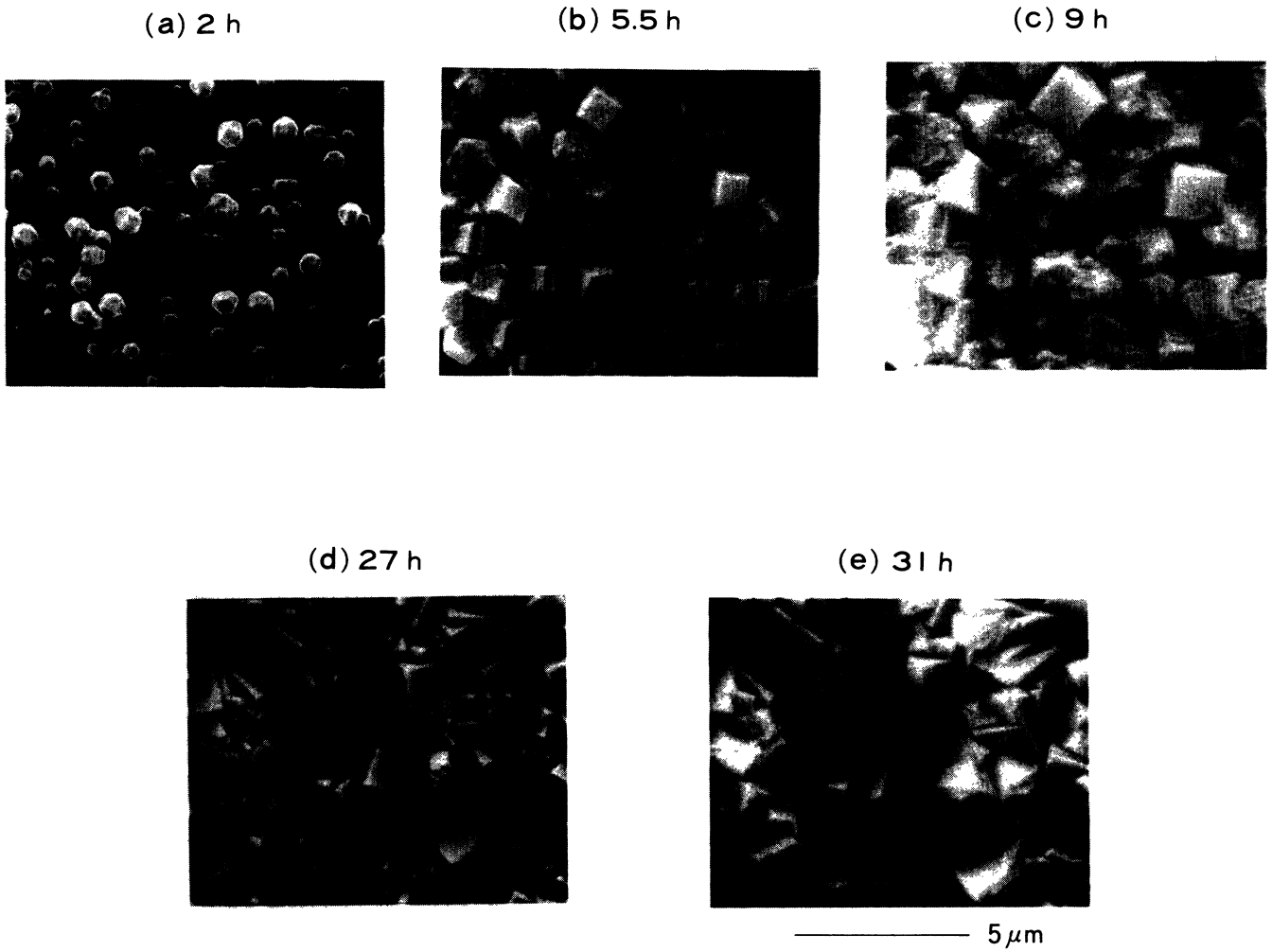

FIG. 16. Growth process for $c = 0.8\%$: (a) after 2 h, (b) after 5.5 h, (c) after 9 h, (d) after 27 h, and (e) after 31 h.

seen in other areas. In the upper right of Fig. 18(a), there are small grains on the side of a large face, which have been "absorbed" into the side as seen in Fig. 18(b). Thus, on the basis of these results and the others discussed so far in this paper, it is concluded that during the CVD synthesis, the following restructuring processes take place at the film surface: (1) increase of the areas of primary diamond faces, (2) overgrowth of small crystallites on well-defined faces, (3) "fusion" of a group of small crystallites to form well-defined larger faces, and finally (4) "absorption" of small crystallites into large faces. Thus, the changes in the surface morphology during CVD are viewed as the result of these "elementary processes" of surface restructuring.

The results obtained in this section is diagrammatically shown in Fig. 19. Initially, diamond particles are formed on the substrate surface, and increase their sizes almost uniformly until the substrate is entirely covered. Then a secondary growth occurs and consequently, a considerably large part of the film surface is covered with small grains. However, well-defined diamond faces are generated almost "suddenly", which is then followed by a higher-order growth of small grains. This cycle is repeated as the CVD synthesis proceeds. The changes in the morphology described above are viewed as a consequence of the "elementary processes" of surface restructuring.

During the observation of the growth at $c = 1.2\%$, an abnormally large grain was found near the edge of the sample, as shown in Fig. 20. Although a group of grains are sitting on top of the large (100) face, roughly 20×20 μm^2 in area, a step structure is clearly visible on the planar area. The step length is about 0.5 μm and the height is about 0.1 μm. Taken together with the previously described results of $c = 0.3\%$, this feature suggests that (100) faces grow by the step growth mechanism. Although no such feature is seen on the (100) faces in the center of the specimen, it is only because the step is too small to be detected by the SEM resolution.

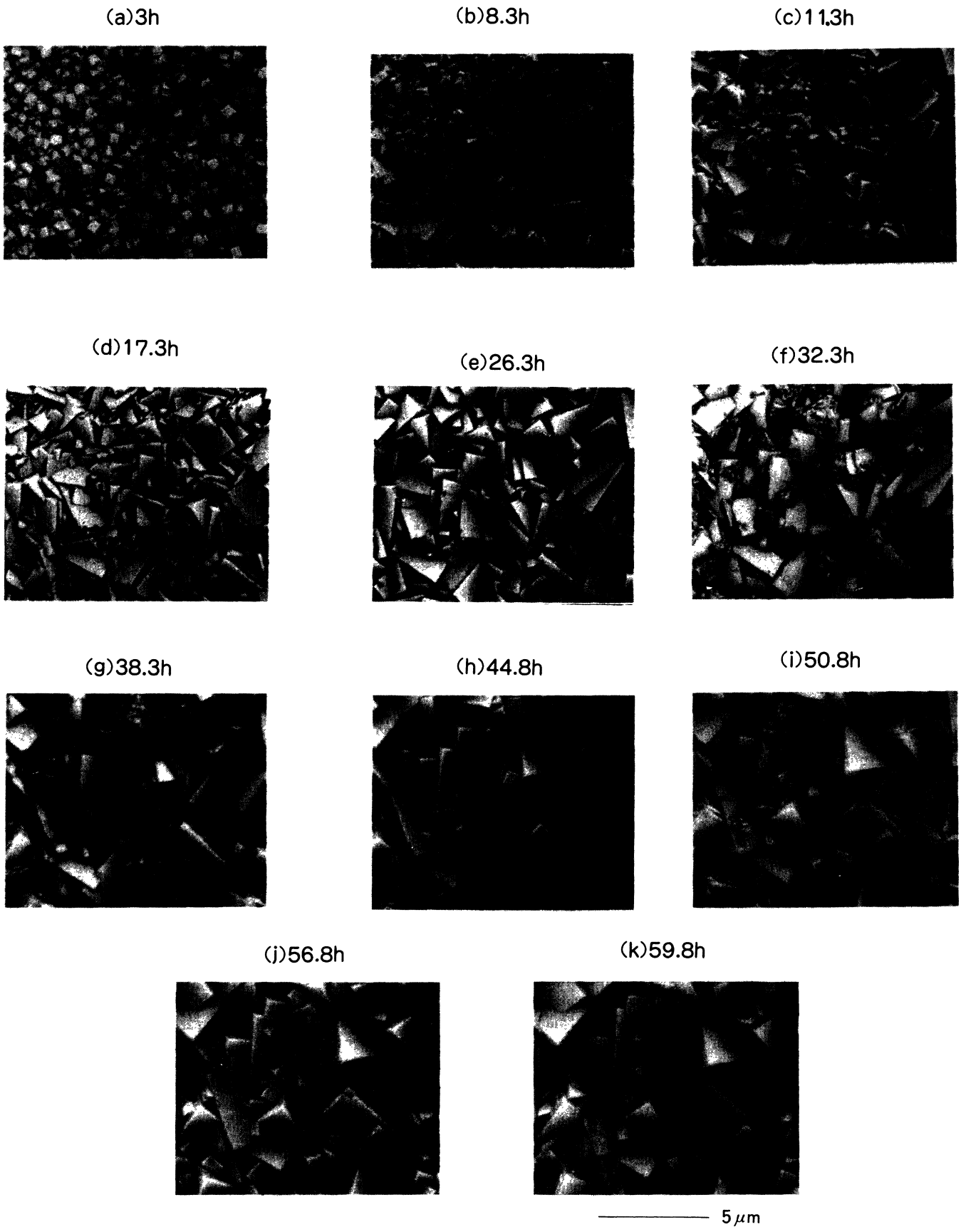

FIG. 17. Growth process for $c = 1.2\%$: (a) after 3 h, (b) after 8.3 h, (c) after 11.3 h, (d) after 17.3 h, (e) after 26.3 h, (f) after 32.3 h, (g) after 38.3 h, (h) after 44.8 h, (i) after 50.8 h, (j) after 56.8 h, and (k) after 59.8 h.

V. DISCUSSION

The major concern related to the morphology of the diamond films described in the present paper is the appearance of square (100) faces. For CH_4 concentrations lower than 0.4%, the faces adjacent to the (100) faces are triangular (111) faces, because the grain shapes comprising the films are cubo-octahedral as seen in Figs. 8(a)–8(c)

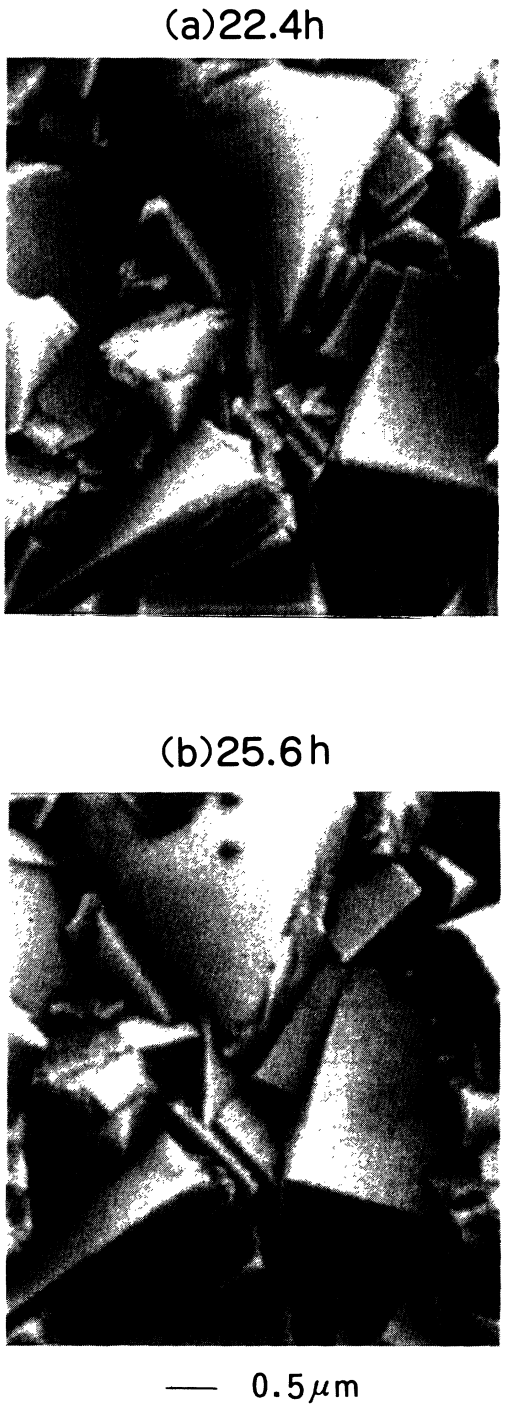

FIG. 18. Restructuring processes for $c = 0.6\%$: (a) after 22.4 h and (b) after 25.6 h.

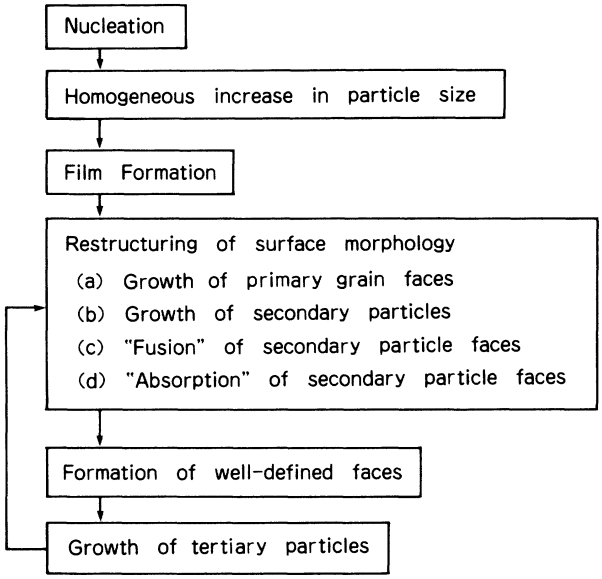

FIG. 19. Growth process of diamond films.

(see also Fig. 1). On the other hand, for concentrations from 0.4% to 1.2%, only (100) faces are seen on the film surfaces. The most striking feature in this case is the fact that the side faces of the (100) faces are rough and no longer exhibit well-defined crystallographic planes within the SEM resolution. Furthermore, the side faces form large angles with the (100) faces, the angles being almost perpendicular to the (100) faces. Thus, it seems that (100) faces result from an anisotropic growth of the film. In what follows, the above results will be considered more closely in order to elucidate the physical implications behind the data.

The appearance of (100) faces on the films is in strong contradiction with the periodic-bond-chain (PBC) theory[60] which successfully describes the morphology of natural diamonds. According to the theory as applied to diamonds, an uninterrupted chain of C—C bonds is called a PCB, and diamond faces are classified into three

FIG. 20. Step structure of the (100) face.

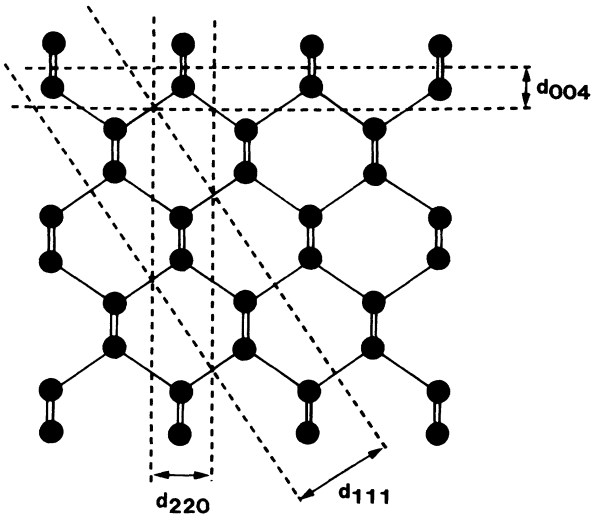

FIG. 21. Projection of the diamond structure along [$\bar{1}$10] (Ref. 60).

groups, *F*, *S*, and *K*, depending on the number of PBC's contained in a surface layer d_{hkl}, as seen in Fig. 21. The *F* (flat) face contains more than two PBC's in a layer d_{hkl}. This face undergoes a layer growth at low carbon supersaturations. The *S* (stepped) face has only one PBC. Finally, the *K* (kinked) face has no PBC, and is predicted to have the highest growth rate, because no nucleation is needed for the growth. The (111), (110), and (100) faces of diamond correspond to the *F*, *S*, and *K* faces, respectively, as shown in Fig. 21. Thus, from the PBC theory combined with a general rule that the faces having the slowest growth rate in the direction normal to the faces determine the crystal morphology, it follows that (100) faces should not appear as diamond facets because of the high growth rate, and even if they appeared, the faces should be rough because they are *K* faces.

It is evident that the above predictions strongly disagree with the experimental data observed here. The (100) faces observed in the present experiment are smooth and flat, apart from the step growth structure (see Figs. 15 and 20). This means that the growth rate of the (100) face is low, particularly for $c > 0.4\%$, in the diamond growth in the microwave plasma. For the facial growth rates v, these data indicate that $v_{100} \sim v_{111} < v_{110}$ for $c < 0.4\%$, and $v_{100} < v_{111}, v_{110}$ for $0.4\% < c < 1.2\%$.

Diamond films synthesized for $0.4\% < c < 1.2\%$ exhibit a unique surface morphology: The film surfaces consist only of (100) faces and which are adjacent to rough surfaces. It seems that this structure arises not only from the fact that the growth rate of (100) is the lowest but also from the fact that (100) faces undergo an unstable growth, because such an anisotropic film structure cannot be accounted for solely by the former reason. However, we are not able to clearly identify the origin of the instability. Presumably, it is related to, firstly, relatively high CH_4 concentrations which might induce a thermodynamic instability due to a high supersaturation of chemically active hydrocarbon species, and secondly, the anisotropy of the environment, for example, the collisional directions of plasma species.

It is interesting to note that Spitsyn *et al.*[24] concluded from their CTR experiments at different temperatures that diamond crystals with a cubic habit appeared at high substrate temperatures, or equivalently, at low supersaturations. This is in contrast to the morphology of diamonds synthesized by HP-HT methods,[61] in which case cubic habit appear at low temperatures. Since the low supersaturation is also equivalent to low hydrocarbon con-

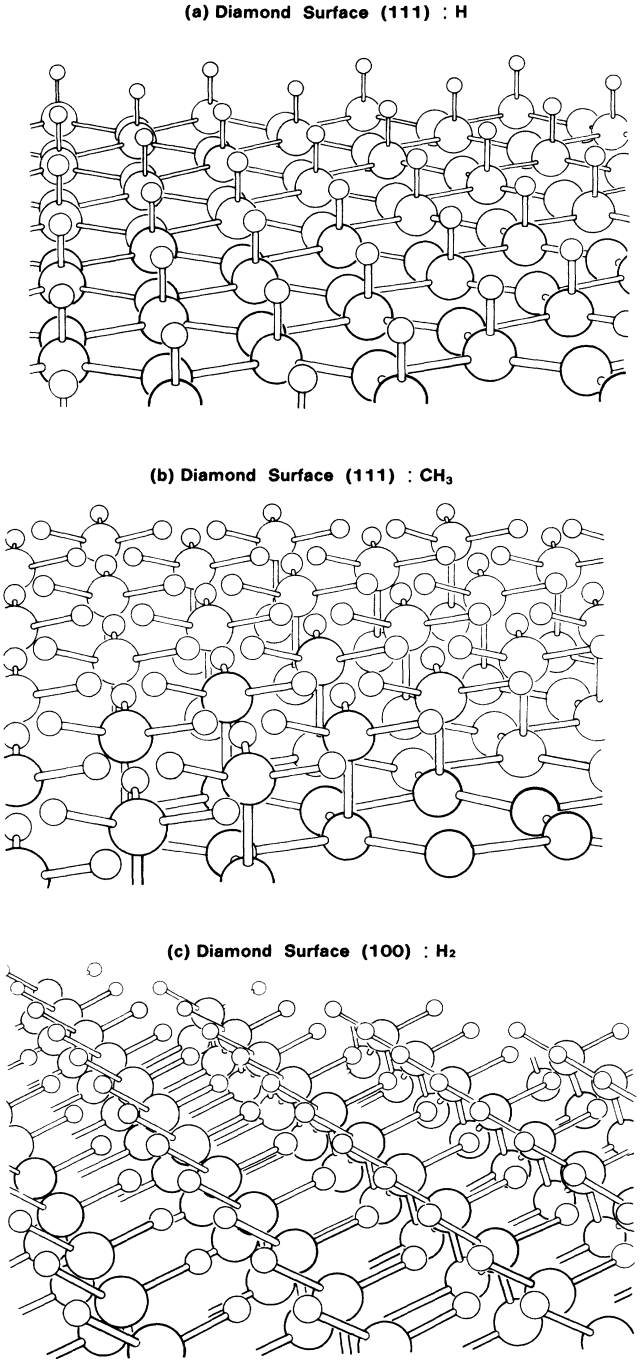

FIG. 22. Schematic structure of hydrogen-chemisorbed diamond surfaces: (a) (111):H, (b) (111):CH_3, and (c) (100):H_2.

centrations, Spitsyn's data is also different from the present results, where (100) faces appear at higher hydrocarbon concentrations. Thus, more detailed investigations are needed to understand these discrepancies.

It is clearly shown in Figs. 15 and 20 that (100) faces grow by the step growth mechanism, and the orientations of the step structures are in conformity with the orientation of the square (100) faces. On the other hand, no step structure was observed on (111) faces. This result is also different from Spitsyn's data[24] in which the step structures are observed both on (100) and (111) faces of large diamond grains and the step orientations are different from the base orientations, exhibiting an initial process of twin structures. Such differences may arise from different experimental methods and conditions.

Figures 22(a)–22(c) show schematically two nonreconstructed (111) surfaces and a (100) surface of diamond chemisorbed by hydrogen atoms, respectively. For the (111) surface, there are two types of surface structures: hydrogen chemisorbed [(111):H] and methyl chemisorbed [(111):CH_3]. In the former case, there is obviously no interference between hydrogen atoms. In the latter case, the possible interference between the adjacent CH_3 groups can be avoided by the rotations of the CH_3 groups about the C—C bonds. On the contrary, for the (100) surface terminated with hydrogen [see Fig. 22(c)], the $H \cdots H$ distance between the adjacent CH_2 groups is only 1.7 Å, which is significantly shorter than the empirical intercore distance of H atoms, i.e., 2.0 Å. Therefore, it seems very unlikely that the nonreconstructed, fully hydrogen-chemisorbed (100) surface shown in Fig. 22(c) really exists, and it is possible that the (100) surface is reconstructed in a similar manner as shown for a hydrogen-chemisorbed Si(100) surface.[62] Thus, the morphological crossover from (111) to (100) at $c=0.4\%$ should be accounted for by the free energies of the (111) and (100) surfaces chemisorbed by hydrogen.

In the study of the film growth presented in Sec. IV, it is seen that the secondary and higher-order growths followed by the conversions to well-defined (100) faces occur periodically with time. Such changes take place concurrently over the entire film surface across the 2×1 cm^2 sample. It seems that there is no reason that such morphological changes should occur coherently over the film surface, because there is no mechanism of cooperativity in the film growth. It may be suspected that the extrinsic effects such as the exposure of the substrate to air and the thermal hysteresis, but not any intrinsic mechanism, cause such changes in the film morphology during the growth. If this is the case, it is to be expected that such extrinsic effects would all the time cause the same change. However, no such change was observed. Therefore, it is concluded that the external perturbations are not attributable to the periodic change in the surface morphology, and that the real cause of the coherency is open for further investigation.

Summarizing the results presented in this paper, diamond films were synthesized for different CH_4 concentrations, and a discrete change in the film morphology was found at $c=0.4\%$ and about 1.2%, as schematically shown in Fig. 9. The films were characterized using x-ray diffraction, RHEED, Raman scattering, and infrared absorption. The evolution of the surface morphology was studied for $c=0.3\%$, 0.8%, and 1.2%, and a general result is schematically shown in Fig. 19. It was found that the morphology of diamond films alternate periodically between the higher-order growth and the conversion to the well-defined surface structure. Such changes are a result of "elementary processes" of restructuring of surface morphology. Similar investigations using different CVD methods would be useful to further understand the growth and morphology of diamond films.

ACKNOWLEDGMENTS

The authors wish to thank Mr. T. Nakatsuka for the SEM photographs. They also thank Dr. K. Inoue, Dr. A. Nakaue, Mr. H. Hayashi, and Mr. A. Morikawa for continuous encouragement. One of the authors (K.K.) also wishes to thank Dr. N. Setaka, Dr. Y. Sato, and Dr. M. Kamo for hospitality and for useful discussions. He further acknowledges Professor R. F. Davis, Dr. J. T. Glass, Professor R. Messier, and Dr. M. Geis for useful discussion.

[1]M. Kamo, S. Matsumoto, Y. Sato, and N. Setaka, U.S. Patent No. 4, 434, 188 (1984).

[2]F. P. Bundy, H. M. Strong, and R. H. Wentorf, Jr., Chem. Phys. Carbon **10**, 213 (1973).

[3]*The Properties of Diamonds,* edited by J. E. Field (Academic, New York, 1979).

[4]R. M. Chrenko and H. M. Strong, GE Corporate Research Report No. 75 CRD 089, 1975 (unpublished).

[5]For thermal conductivity of diamond films, see A. Ono, T. Baba, H. Funamoto, and A. Nishikawa, Jpn. J. Appl. Phys. **25**, L808 (1986).

[6]N. Fujimori, T. Imai, and A. Doi, Vacuum **36**, 99 (1986).

[7]W. G. Eversole, U.S. Patents No. 3,030,187 and No. 3,030,188 (April 1962).

[8]B. V. Derjagin, D. V. Fedoseev, V. M. Lukyanovich, B. V. Spitzin, V. A. Ryabov, and A. V. Lavrentyev, J. Cryst. Growth **2**, 380 (1968).

[9]B. V. Deryagin, L. L. Builov, V. M. Zubkov, A. A. Kochergina, and D. V. Fedoseev, Kristallografiya **14**, 535 (1969) [Sov. Phys.—Crystallogr. **14**, 449 (1969)].

[10]B. V. Deryagin, D. V. Fedoseev, V. M. Luk'yanovich, B. V. Spitzin, V. A. Ryabov, and A. V. Lavrent'ev, Dokl. Akad. Nauk SSSR **181**, 1094 (1968) [Sov. Phys.—Dokl. **13**, 783 (1969)].

[11]B. V. Deryagin, V. G. Lyuttsau, D. V. Fedoseev, and V. A. Ryabov, Dokl. Akad. Nauk SSSR **190**, 86 (1970) [Sov. Phys.—Dokl. **15**, 58 (1970)].

[12]B. V. Deryagin and D. V. Fedoseev, Russ. Chem. Rev. **39**, 783 (1970).

[13]D. V. Fedoseev, V. P. Varnin, and B. V. Deryaguin, Dokl.

Akad. Nauk SSSR **193**, 1290 (1970) [Sov. Phys.—Dokl. **15**, 787 (1971)].
[14]B. V. Derjaguin and D. V. Fedoseev, Carbon **11**, 299 (1973).
[15]B. V. Deryaguin and D. V. Fedoseev, Dokl. Akad. Nauk SSSR **213**, 1304 (1973) [Sov. Phys.—Dokl. **18**, 771 (1974)].
[16]B. V. Deryagin, B. V. Spitsyn, A. E. Aleksenko, A. E. Gorodestkii, A. P. Zakharov, and R. I. Nazarova Dokl. Akad. Nauk SSSR **213**, 1059 (1973) [Sov. Phys.—Dokl. **18**, 822 (1974)].
[17]B. V. Derjaguin and D. B. Fedoseev, Sci. Am. **233**(5), 102 (1975).
[18]B. V. Deryaguin, D. V. Fedoseev, V. P. Varnin, A. E. Gorodetskii, A. P. Zakharov, and I. G. Teremetskaya, Zh. Eksp. Teor. Fiz. **69**, 1250 (1975) [Sov. Phys.—JETP **42**, 639 (1975)].
[19]B. V. Deryagin, D. V. Fedoseev, N. D. Polyanskaya, and E. V. Statenkova Krystallografiya **21**, 433 (1976) [Sov. Phys.—Crystallogr. **21**, 239 (1976)].
[20]D. V. Fedoseev, S. P. Vnukov, and B. V. Deryagin, Russ. Zh. Fiz. Khim. **50**, 2751 (1976) [J. Phys. Chem. **50**, 1645 (1976)].
[21]B. V. Deryagin, B. V. Spitsyn, L. L. Builov, A. A. Klochkov, A. E. Gorodetskii, and A. V. Smol'yaninov, Dokl. Akad. Nauk SSSR **231**, 333 (1976) [Sov. Phys.—Dokl. **21**, 676 (1976)].
[22]V. P. Varnin, B. V. Deryaguin, D. V. Fedoseev, I. G. Teremetskaya, and A. N. Khodan, Kristallografiya **22**, 893 (1977) [Sov. Phys.—Crystallogr. **22**, 513 (1977)].
[23]D. V. Fedoseev, B. V. Deryaguin, I. G. Varshavskaya, A. V. Lavrent'ev, and V. V. Matveev, Zh. Eksp. Teor. Fiz. **80**, 413 (1981) [Sov. Phys.—JETP **53**, 210 (1981)].
[24]B. V. Spitsyn, L. L. Bouilov, and B. V. Derjaguin, J. Cryst. Growth **52**, 219 (1981).
[25]P. V. Fedoseev, V. P. Varnin, Zh. Fiz. Khim. **57**, 2726 (1983) [Russ. J. Phys. Chem. **57**, 1647 (1983)].
[26]D. V. Fedoseev, V. P. Varnin, and B. V. Deryagin, Russ. Chem. Rev. **53**, 435 (1984).
[27]J. C. Angus, H. A. Will, and W. S. Stanko, J. Appl. Phys. **39**, 2915 (1968).
[28]J. C. Angus and N. C. Gardner, U.S. Patent No. 3,661,526 (1972).
[29]M. Sokolowski, A. Sokolowska, B. Gokieli, A. Michalski, A. Rusek, and Z. Romanovski, J. Cryst. Growth **47**, 421 (1979).
[30]R. Mania, L. Stobierski, and R. Pampuch, Cryst. Res. Tech. **16**, 785 (1981).
[31]N. Setaka, National Institute for Research in Inorganic Materials, Research Reports No. 20, 1979, and No. 39, 1984 (unpublished).
[32]S. Matsumoto, Y. Sato, M. Tsutsumi, and N. Setaka, J. Mater. Sci. **17**, 3106 (1982).
[33]S. Matsumoto, Y. Sato, M. Kamo, and N. Setaka, Jpn. J. Appl. Phys. **21**, L183 (1982).
[34]S. Matsumoto and Y. Matsui, J. Mater. Sci. **18**, 1785 (1983).
[35]M. Kamo, Y. Sato, S. Matsumoto, and N. Setaka, J. Cryst. Growth **62**, 642 (1983).
[36]S. Matsumoto, J. Mater. Sci. Lett. **4**, 600 (1985).
[37]N. Setaka, Hyomen (Surface) **22**, 110 (1984) (in Japanese).
[38]M. Tsuda, M. Nakajima, and S. Oikawa, J. Am. Chem. Soc. **108**, 5780 (1986).
[39]M. Tsuda, M. Nakajima, and S. Oikawa, Jpn. J. Appl. Phys. **26**, L527 (1987).
[40]Y. Hirose and Y. Terasawa, Jpn. J. Appl. Phys. **25**, L519 (1986).
[41]A. Sawabe and T. Inuzuka, Thin Solid Films **137**, 89 (1986).
[42]A. Sawabe and T. Inuzuka, Appl. Phys. Lett. **46**, 146 (1985).
[43]K. Tachibana, M. Nishida, H. Harima, and Y. Urano, J. Phys. D **17**, 1727 (1984).
[44]O. Matsumoto, H. Toshima, and Y. Kanzaki, Thin Solid Films **128**, 341 (1985).
[45]Y. Sato, S. Matsuda, and S. Nogita, J. Mater. Sci. Lett. **5**, 565 (1986).
[46]O. Matsumoto and T. Katagiri, Thin Solid Films **146**, 283 (1987).
[47]R. Messier, J. Vac. Sci. Technol. A **4**, 490 (1986).
[48]Y. Sato (private communication).
[49]N. Wada and S. A. Solin, Physica B + C **105B**, 353 (1981).
[50]S. A. Solin and A. K. Ramdas, Phys. Rev. B **1**, 1687 (1970).
[51]R. O. Dillon, J. A. Woolam, and V. Katkanant, Phys. Rev. B **29**, 3482 (1984).
[52]H. Ishida, H. Fukuda, G. Katagiri, and A. Ishitani, Appl. Spectros. **40**, 322 (1986).
[53]F. Tuinstra and J. L. Koenig, J. Chem. Phys. **53**, 1126 (1970).
[54]H. Shirakawa, T. Ito, and S. Ikeda, Polymer J. **4**, 460 (1973).
[55]A. Baruya, Macromolecules **16**, 578 (1983).
[56]B. Discher, A. Bubenzer, and P. Koidl, Solid State Commun. **48**, 105 (1983).
[57]T. Miyasato, Y. Kawakami, T. Kawano, and A. Hiraki, Jpn. J. Appl. Phys. **23**, L234 (1984).
[58]K. Nakazawa, S. Ueda, M. Kumeda, A. Morimoto, and T. Shimizu, Jpn. J. Appl. Phys. **21**, L176 (1982).
[59]Y. Sato (private communication), and see also S. Matsumoto, Y. Sato, and N. Setaka, Carbon **19**, 232 (1981).
[60]P. Hartman, *Crystal Growth: An Introduction,* edited by P. Hartman (North-Holland, Amsterdam, 1973), p. 367.
[61]I. Sunagawa, J. Jpn. Assoc. Mineral. Petrol. Econ. Geol. Special Issue **3**, 129 (1982).
[62]T. Sakurai and H. Hagstrum, Phys. Rev. B **14**, 1593 (1976).

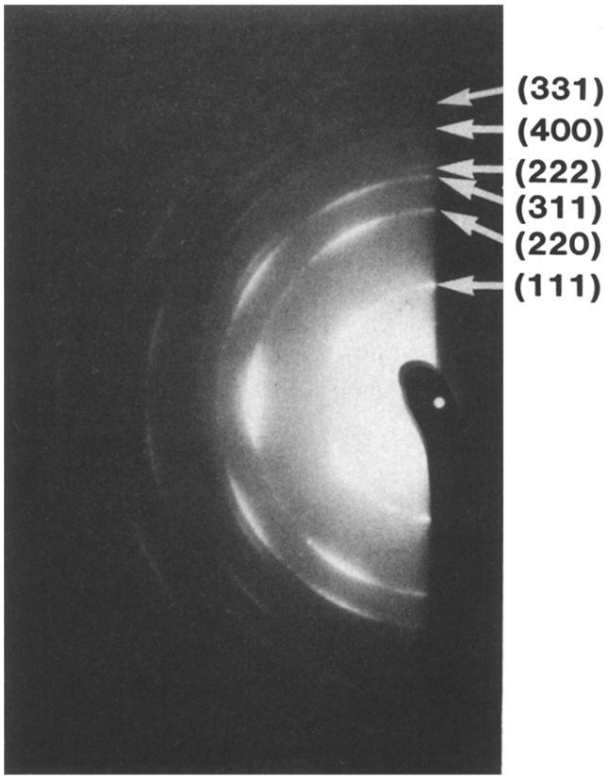

FIG. 11. RHEED pattern of a diamond film deposited on a Si(111) substrate at $c = 1.0\%$ for 7 h. The lattice spacings evaluated from the pattern are listed in Table I.

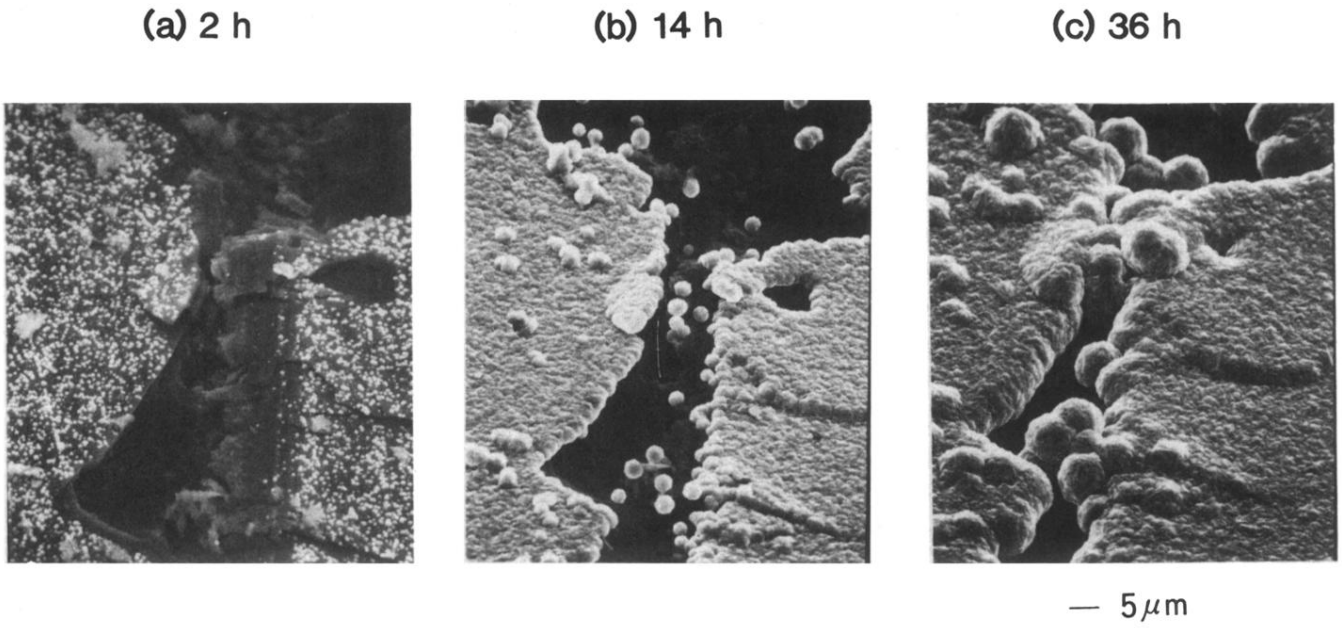

FIG. 14. Overview of a formation process of diamond film: (a) after 3 h, (b) after 12 h, and (c) after 30 h. The substrate is Si polished with a diamond paste. The dark area in the center is a scratch mark given on the substrate before the synthesis, and it is seen that the nucleation density of diamond particles is very low on the fresh Si surface.

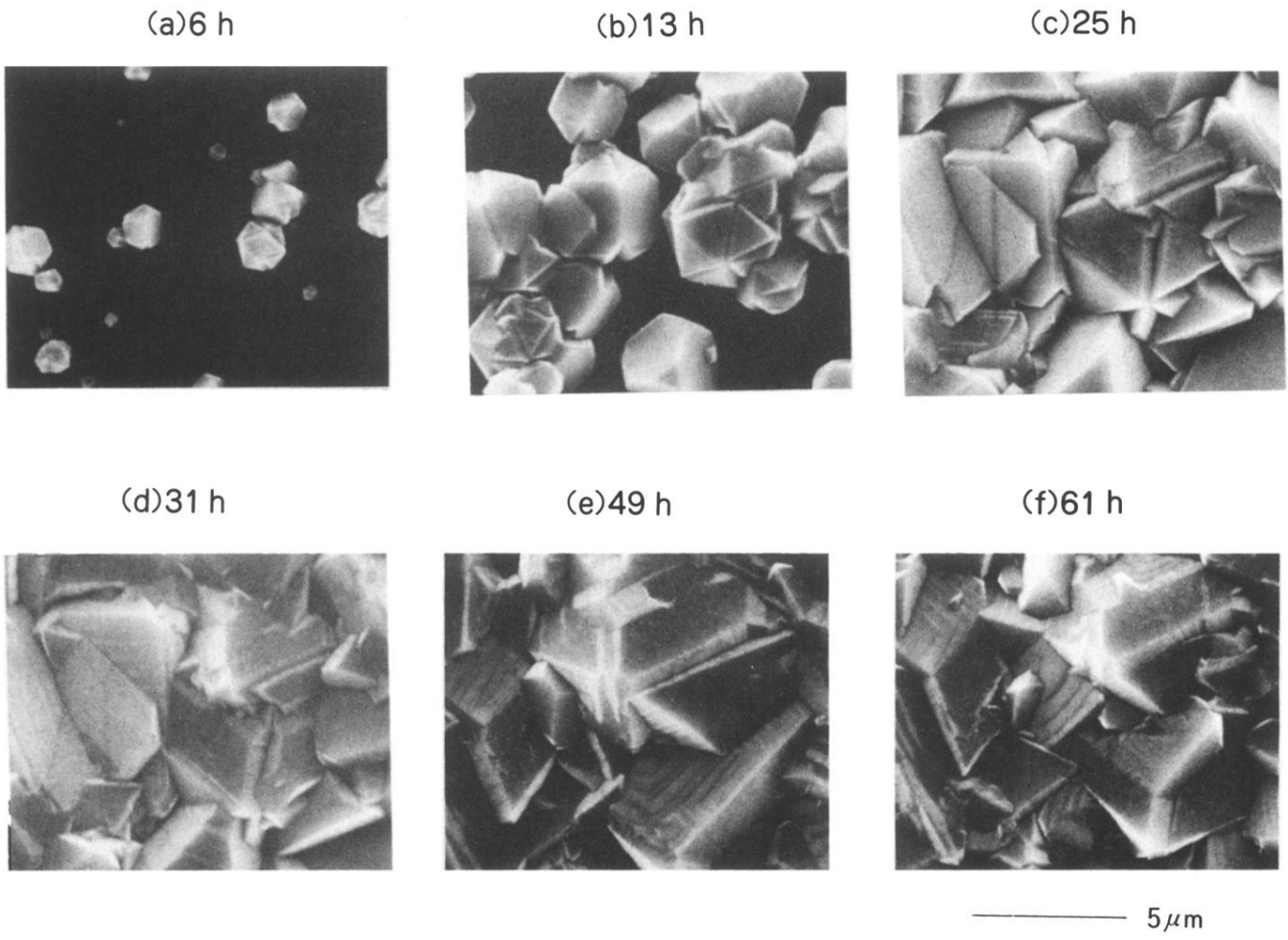

FIG. 15. Growth process for $c = 0.3\%$: (a) after 6 h, (b) after 13 h, (c) after 25 h, (d) after 31 h, (e) after 49 h, and (f) after 61 h.

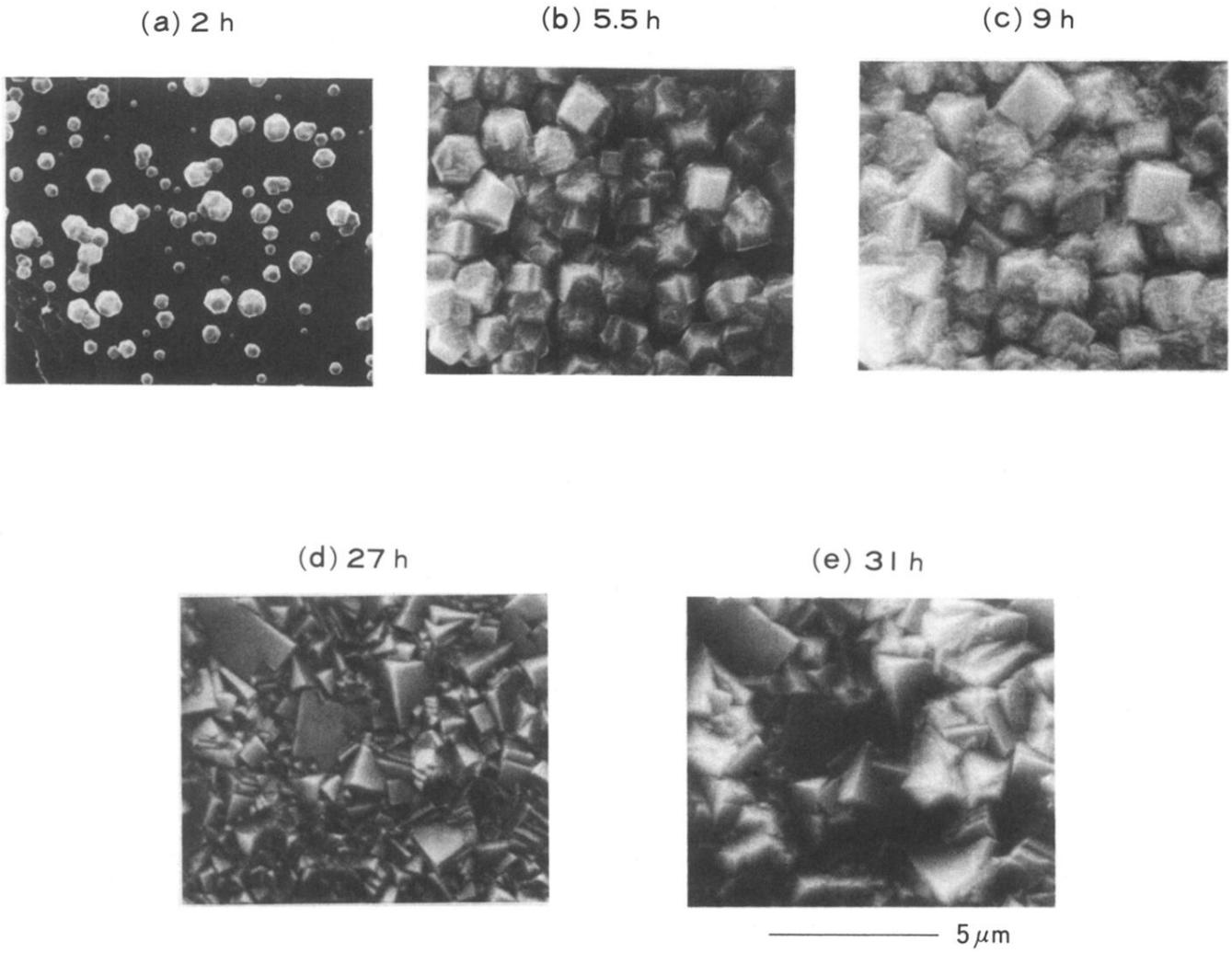

FIG. 16. Growth process for $c = 0.8\%$: (a) after 2 h, (b) after 5.5 h, (c) after 9 h, (d) after 27 h, and (e) after 31 h.

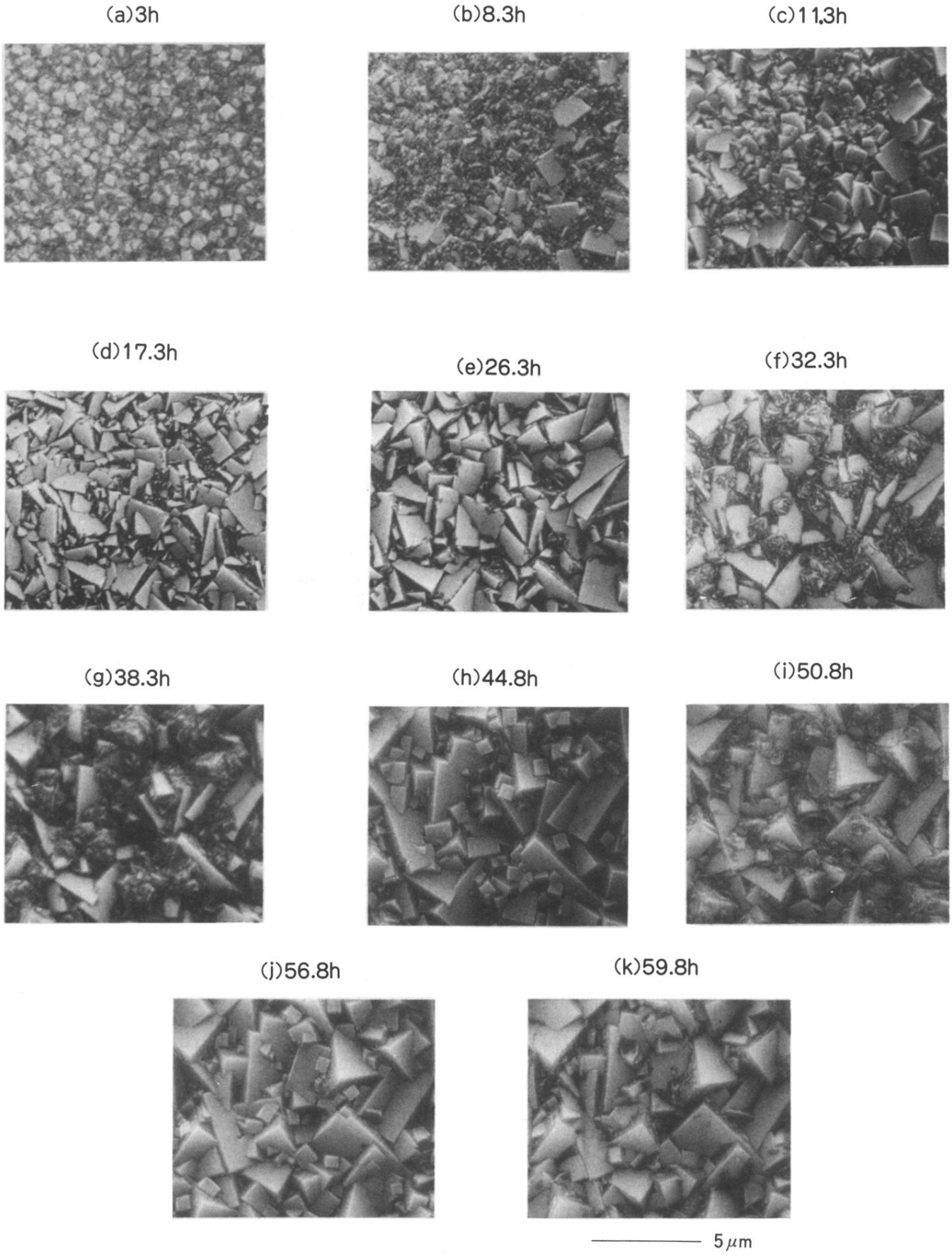

FIG. 17. Growth process for $c = 1.2\%$: (a) after 3 h, (b) after 8.3 h, (c) after 11.3 h, (d) after 17.3 h, (e) after 26.3 h, (f) after 32.3 h, (g) after 38.3 h, (h) after 44.8 h, (i) after 50.8 h, (j) after 56.8 h, and (k) after 59.8 h.

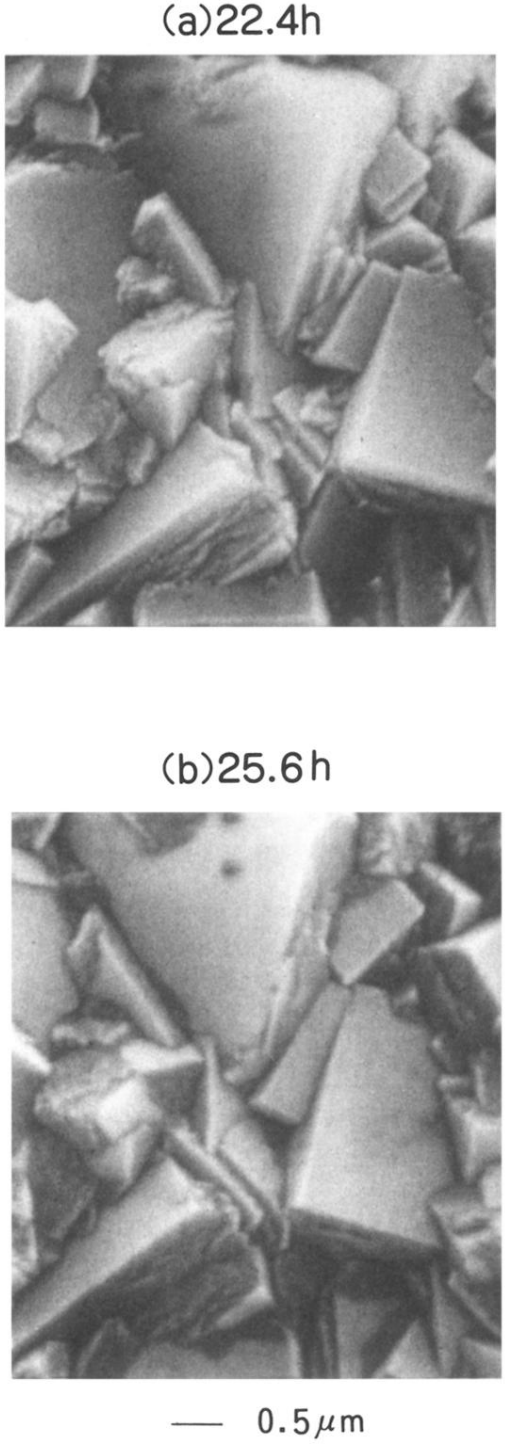

FIG. 18. Restructuring processes for $c = 0.6\%$: (a) after 22.4 h and (b) after 25.6 h.

FIG. 20. Step structure of the (100) face.

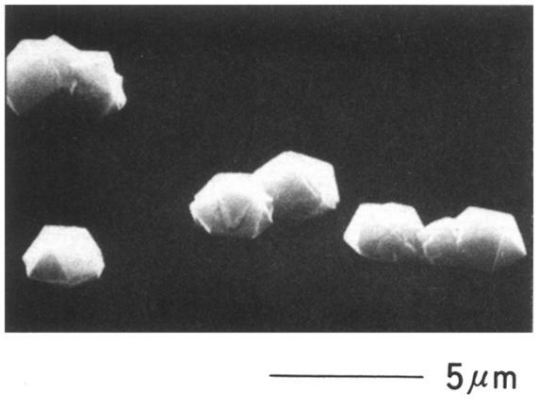

FIG. 3. Diamond particles grown on si substrate.

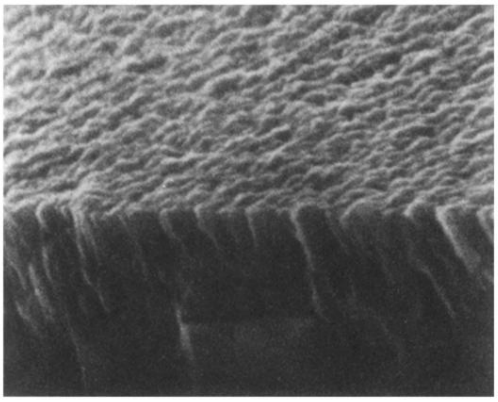

FIG. 4. A broken edge of a polycrystalline diamond film grown on a Si substrate at the CH_4 concentration $c = 1$ vol % for 7 h. Note that the film exhibits a columnar growth.

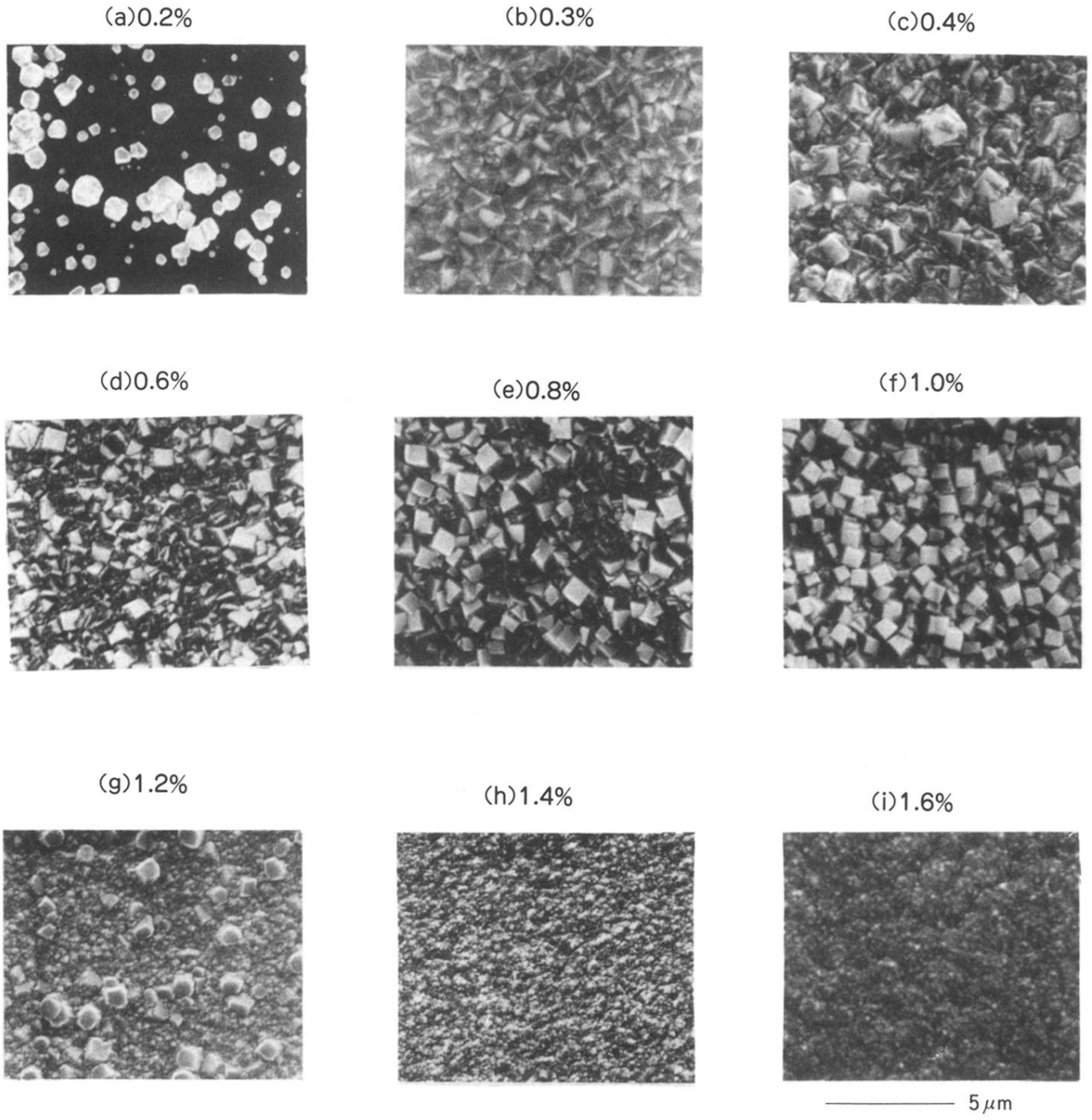

FIG. 8. Surface morphology of the diamond films observed by SEM: (a) 0.2%, (b) 0.3%, (c) 0.4%, (d) 0.6%, (e) 0.8%, (f) 1.0%, (g) 1.2%, (h) 1.4%, and (i) 1.6%. The films are deposited on Si(100) for 7 h.

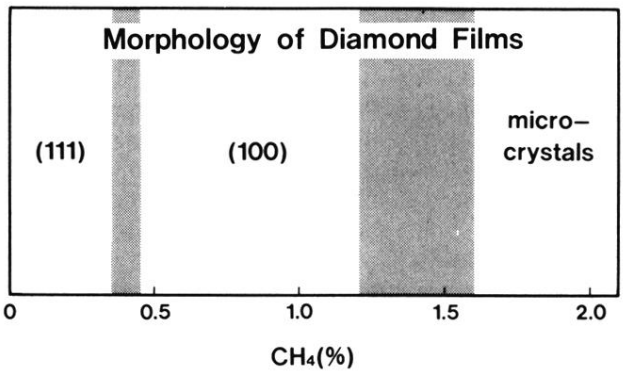

FIG. 9. Morphology of the diamond films with respect to the CH_4 concentration.